
Progress and limitations of deep networks to recognize objects in unusual poses

Amro Abbas

The African Institute For Mathematical Sciences
afagiri@aimsammi.org

Stéphane Deny

Aalto University
stephane.deny@aalto.fi

Abstract

Deep networks should be robust to rare events if they are to be successfully deployed in high-stakes real-world applications (e.g., self-driving cars). Here we study the capability of deep networks to recognize objects in unusual poses. We create a synthetic dataset of images of objects in unusual orientations, and evaluate the robustness of a collection of 38 recent and competitive deep networks for image classification. We show that classifying these images is still a challenge for all networks tested, with an average accuracy drop of 29.5% compared to when the objects are presented upright. This brittleness is largely unaffected by various network design choices, such as training losses (e.g., supervised vs. self-supervised), architectures (e.g., convolutional networks vs. transformers), dataset modalities (e.g., images vs. image-text pairs), and data-augmentation schemes. However, networks trained on very large datasets substantially outperform others, with the best network tested—Noisy Student EfficientNet-L2 trained on JFT-300M—showing a relatively small accuracy drop of only 14.5% on unusual poses. Nevertheless, a visual inspection of the failures of Noisy Student reveals a remaining gap in robustness with the human visual system. Furthermore, combining multiple object transformations—3D-rotations and scaling—further degrades the performance of all networks. Altogether, our results provide another measurement of the robustness of deep networks that is important to consider when using them in the real world. Code and datasets are available at <https://github.com/amro-kamal/ObjectPose>.

1 Introduction

A considerable effort has been made in the past decade to develop deep neural networks that could see as well as humans. These networks, when they are tested on in-distribution test sets, achieve or even exceed human-level performance. For example, FlorenceNet (Yuan et al., 2021) and Meta Pseudo Labels (Pham et al., 2021) achieve less than 2% top-5 error on ImageNet, outperforming an expert human with 5.1% top-5 error (Russakovsky et al., 2015). However, in real-world applications, deep networks are often deployed and used to detect harder examples than those seen in the development test set. This has led researchers to investigate the performance of networks using more challenging test examples, in the so-called out-of-distribution (OOD) regime (Hendrycks et al., 2021b; Hendrycks and Dietterich, 2019; Hendrycks et al., 2021a; Wang et al., 2019; Dodge and Karam, 2017; Recht et al., 2019a; Shankar et al., 2021; Geirhos et al., 2018, 2021). Many of the previous studies on out-of-distribution generalization have focused on measuring the generalization capabilities of networks to distorted images. Notably, Geirhos et al. (2021) show that the newest generation of very large deep networks is closing the human-machine robustness gap on 17 different out-of-distribution image distortion types. However, most of the transformations used to generate these datasets are local distortions that only affect the texture of objects, but do not change the global structure of the image. Taori et al. (2020) shows that robustness to these kinds of distortions does not transfer entirely to natural shifts and does not represent a comprehensive measure of the network’s robustness.



Figure 1: Random samples from our custom dataset ObjectPose, designed to probe deep networks’ robustness to unusual poses. For each of the 17 objects composing the dataset, background and orientation are systematically varied to generate the full dataset. The 17 object categories in ObjectPose are ‘airliner’, ‘barber chair’, ‘cannon’, ‘fire engine’, ‘folding chair’, ‘forklift’, ‘garbage truck’, ‘hammerhead shark’, ‘jeep’, ‘mountain bike’, ‘park bench’, ‘rocking chair’, ‘shopping cart’, ‘table lamp’, ‘tank’, ‘tractor’, and ‘wheel barrow’.

Pose transformations (e.g., a bus seen upside-down) represent an interesting case-study for networks’ robustness, as (1) unlike simple distortions, these transformations affect the global structure of the image, and (2) it would be technically challenging to augment an image dataset at scale with this type of 3D transformations. In a rare study of its kind, Alcorn et al. (2019) show that two deep networks, Inception-V3 (Szegedy et al., 2016) and ResNet50 (He et al., 2016), drastically fail to recognize objects in unusual poses, incorrectly classifying most of the poses explored. Later, Madan et al. (2021) also reveal a brittleness of ResNet18 and CLIP (Radford et al., 2021) to small changes in pose, in an adversarial setting.

In this study, we revisit the question of networks’ robustness to unusual poses using a diverse set of the latest and best publicly available networks for image classification. We test 38 networks with a variety of different architectures, sizes, training datasets, and training objectives on a custom dataset of images of objects in unusual poses. Our contributions are:

- We observe that, on unusual poses, the networks of our collection suffer from a 14.5% to 45.5% accuracy drop compared to usual poses. A visual inspection of networks’ failures reveal that, even for the best models, a robustness gap remains with the human visual system.
- We provide a detailed study of the effect of in-(image)-plane vs. out-of-plane object rotations, background-foreground congruency, and rotation angle on performance. We show that the best networks rely on a different strategy than weaker networks when it comes to incorporating information from the background.
- By combining multiple unusual transformations—such as object rotations and scaling—we show that such combinations lead to further performance degradation for all networks, as predicted by a combinatorial model of error.
- In an effort to go beyond synthetic datasets, we test the networks on images from the *Common Objects in 3D Dataset* (CO3D), a dataset of objects seen in various poses, and show a generalization gap of 5.2% on average across networks compared to a benchmark of objects presented in their usual pose, ImageNetV2.
- We make our custom datasets, deep network collection and code available publicly on Github¹ for future investigations by the community.

2 Dataset and Networks

ObjectPose Dataset We generated a synthetic dataset of objects in unusual poses, ObjectPose (Fig. 1, all details in Appendix A). The dataset contains 27,540 images of 17 high-quality 3D objects—each belonging to one of 1000 ImageNet (Russakovsky et al., 2015) classes—rendered in a range of different orientations and over different background images, following the pipeline of (Alcorn et al., 2019). Briefly, the object is first placed in an initial upright position. We then choose one of the *YAW*, *ROLL*, or *PITCH* axes to rotate the object along it, and render it on top of a background image. We used three different background images with each object. Two of the backgrounds are images chosen manually from the internet to match the object’s usual context and not to contain any other ImageNet object. We chose the third background to be grey with all its RGB pixel values equal to (0.485, 0.456, 0.406), corresponding to the average pixel color of ImageNet images. In order to focus on robustness to unusual poses, each object is chosen carefully so that the resulting images for that object are correctly classified with >90% accuracy by a ResNet-50 when the object’s orientation is less than 10° apart from its upright pose. We gather these images where the object is rotated by -10° to 10° only in the ObjectPose +-10 dataset (1,683 images in total), and exclude them from ObjectPose, such that ObjectPose only contains unusual poses (11° to 349° from the upright pose).

Deep Networks We tested a collection of 38 networks on ObjectPose (all details in Appendix B and suppl. table 1). We chose a diverse set of networks with different architectures, training datasets sizes, number of parameters, and training objectives. The networks have varying number of parameters (from 22M up to 645M), and different architectures including convolutional neural networks (CNNs) (He et al., 2016; Xie et al., 2020; Kolesnikov et al., 2020; Chen et al., 2020b; Liu et al., 2022), Vision Transformers (ViTs) (Dosovitskiy et al., 2020; Chen et al., 2021; Liu et al., 2021) (Bao et al., 2021; Touvron et al., 2021), and MLP-Mixers (Tolstikhin et al., 2021). We also include ConViT (d’Ascoli et al., 2021), a hybrid CNN-ViT architecture that adds a convolutional inductive bias to the Vision Transformer.

We chose networks trained under different objectives, including:

- Supervised learning, including convolutional architectures, such as (He et al., 2016; Xie et al., 2020; Liu et al., 2022; Kolesnikov et al., 2020), Vision Transformers, such as (Dosovitskiy et al., 2020; Chen et al., 2021; Bao et al., 2021; Touvron et al., 2021; Liu et al., 2021, 2022), and MLP-mixer (Tolstikhin et al., 2021),
- Self-supervised learning, such as SimCLR (Chen et al., 2020a), and BEiT (Bao et al., 2021),
- Semi-weakly supervised learning, such as SWSL-ResNet50 and SWSL-ResNeXt101 (Chen et al., 2020b), and weakly supervised learning, such as SWAG (Singh et al., 2022),
- Text supervision, such as CLIP (Radford et al., 2021).

¹<https://github.com/amro-kamal/ObjectPose>

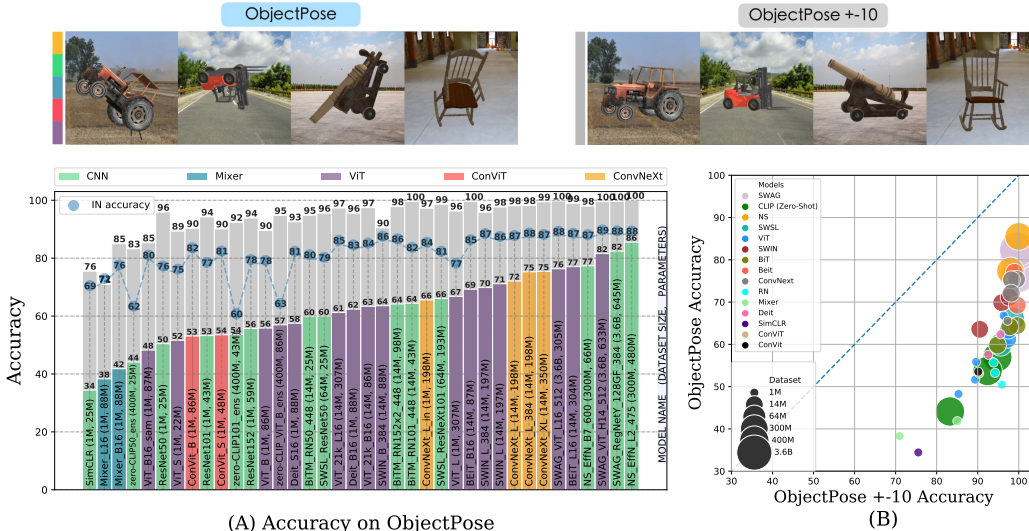


Figure 2: **Performance of all networks on ObjectPose.** (A) Rotating the objects in unusual poses (ObjectPose, colored bars) induces a top-1 accuracy drop of 14.5%-45.5% compared to when objects are presented upright (ObjectPose +10, grey bars). Bar colors indicate different architectures. Blue dots: Top-1 accuracy on ImageNet (as reported in the papers). (B) **Accuracy on usual vs. unusual poses.** Networks trained on ImageNet1k cluster together with low accuracy on ObjectPose. Networks trained on ImageNet21k perform better, and networks trained on extremely large datasets—Noisy Student models (300M images) and SWAG (3.6B images)—perform the best, with the exception of CLIP models (400M images), which were not fine-tuned on ImageNet categories.

The networks were trained on datasets with different sizes ranging from 1M to 3.6B images. Among the networks we use, Noisy Student EfficientNet (Xie et al., 2020) (300M images) and SWAG (Singh et al., 2022) (3.6B images) are the only networks pretrained on extremely large datasets and fine-tuned on ImageNet. Although CLIP (Radford et al., 2021) was pretrained on a very large dataset (400M image-caption examples), it was not fine-tuned on ImageNet.

The best network of our collection according to its performance on ImageNet is the SWAG-RegNetY-128GF-384 model (Singh et al., 2022), pretrained with a weakly-supervised learning approach on 3.6B Instagram images (IG). It achieves 88.55% ImageNet top-1 accuracy.

We also include networks trained using special optimizers such as the ViT-B16-SAM model (Chen et al., 2021), a vision transformer trained with the recently proposed sharpness-aware minimization optimizer (SAM) (Foret et al., 2020), which is designed to improve generalization and robustness.

3 Results

All networks exhibit a performance drop on unusual poses compared to usual poses (Fig. 2). We measure networks’ robustness to unusual object poses by testing their accuracy on our synthetic dataset, ObjectPose. Our collection of networks show a top-1 accuracy drop in a range 14.5%-45.5% on unusual poses compared to usual poses (ObjectPose +10). Examples of network failures are shown in Fig. 3 for the best model tested Noisy Student EfficientNet-L2, and in suppl. fig. 17 for another high-performing model, BEiT-B/16.

Scaling both training dataset size and network capacity is helpful on ObjectPose. Networks trained on larger datasets show a narrower performance gap than networks trained on smaller datasets (Fig. 2B), with the exception of CLIP models which were not fine-tuned on ImageNet categories. It is also important for the network to have a sufficient size (i.e. number of parameters) to benefit from the large dataset. This is deduced by the performance of the EfficientNet-L2 model (480M parameters) compared to EfficientNet-B7 (66M parameters), both trained using the Noisy Student method on the JFT-300M dataset. While EfficientNet-L2 outperforms the rest of the networks on ObjectPose, EfficientNet-B7 performs on par with many networks pretrained on smaller datasets



Figure 3: Selected failures of Noisy Student EfficientNet-L2—the best-performing network of our collection—on ObjectPose. Left column: Objects presented upright and top-5 predictions from the network (as measured by the softmax layer activations). Other columns: Objects presented in incorrectly classified poses and top-5 predictions from the network. Some of these errors reveal a brittleness compared to the human visual system (e.g., a tank at 90° is confused with a shield).

(such as ImageNet21k). Although SWAG models are pretrained on more images (3.6B) and have more parameters, they do not outperform Noisy Student EfficientNet-L2. This also shows that scaling the dataset is not the only factor that matters, here the training procedure and architecture also play an important role (see appendix B for individual networks’ descriptions). In particular, Noisy student was trained using the RangAugment data augmentation method (Cubuk et al., 2020) which applies intensive data augmentation including rotations and shears. In contrast, SWAG only used a limited augmentation strategy of cropping and flipping and not including rotations and shears. Lastly, in Appendix C.2, we show that carefully engineering the textual prompts to CLIP to suggest that the object is in an unusual pose can slightly improve this model’s performance.

A visual inspection of networks’ failures reveals room for improvement even for the best networks tested (Fig. 3). By visually inspecting the errors made by the networks (Fig. 3 and suppl. figures 17-24 at the end of the appendix), we find that even the best model tested, Noisy Student EfficientNet-L2 (NS), makes errors that a human observer would not. On some objects, such as the forklift in suppl. fig. 18, we see that NS performs amazingly well in all orientations, unlike models trained on smaller datasets such as BiTM (suppl. fig. 23). On other examples, such as the hammerhead shark in poses where we cannot see the hammerhead (suppl. fig. 19), NS makes errors that a human observer would certainly make as well, confusing the hammerhead shark with another type of shark. But some errors made by NS reveal a brittleness compared to our visual system. For example, in suppl. fig. 20, NS confuses a bicycle with a unicycle in many poses; in suppl. fig. 21, NS confuses a canon at 90° with a harp or a guillotine, and in suppl. fig. 22 a chair with a plow. In conclusion, none of these networks performs perfectly, and even the best networks tested make errors that would probably be avoided by a human.

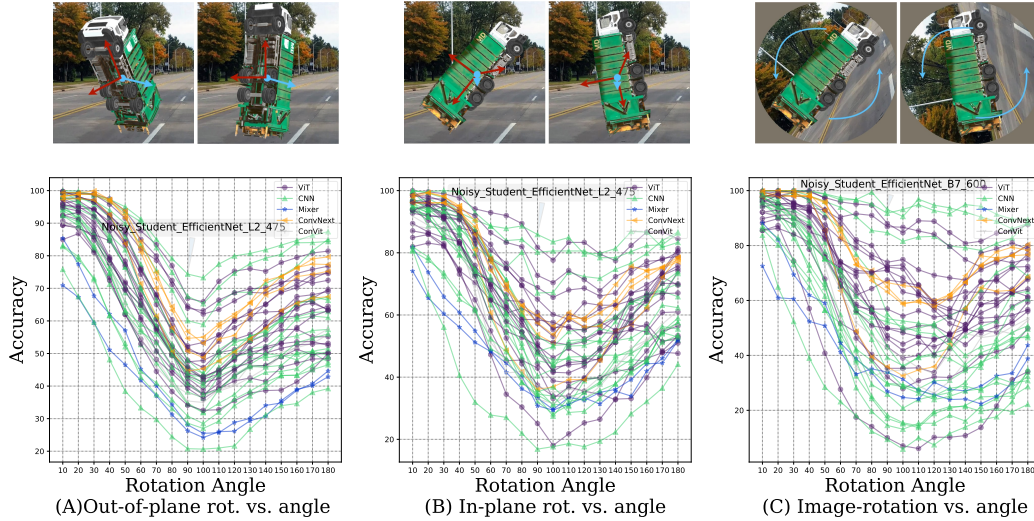
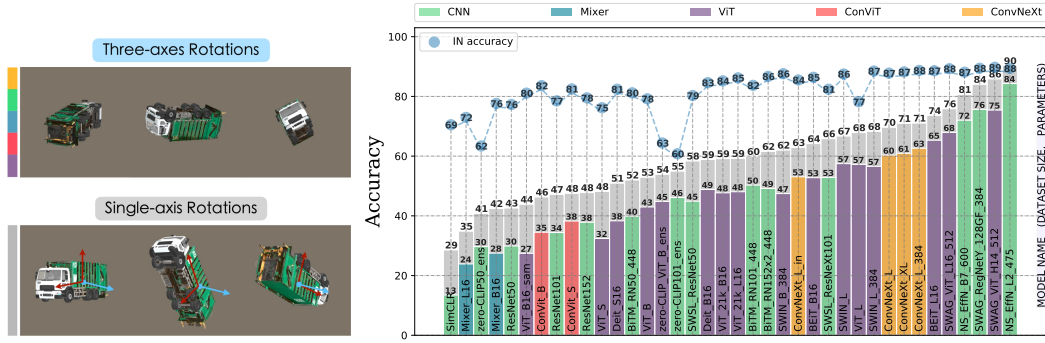


Figure 5: Accuracy decreases as we increase rotation angle, with a low point at 90° . Networks are less robust to (A) out-of-plane rotations than (B) in-plane rotations and (C) image rotations. Noisy Student EfficientNet models are very robust to image rotations, perhaps for the reason that they were trained with this type of augmentation (RandAugment). Yet they are not completely robust to the two other types of rotations.

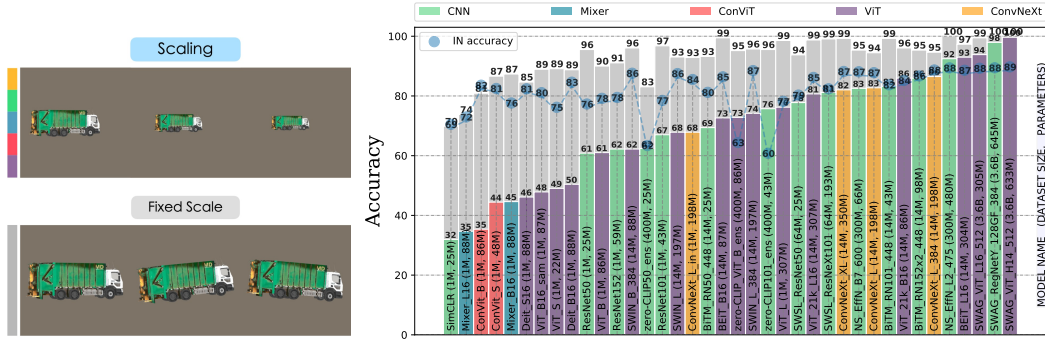
type of data augmentation is not enough to guarantee full robustness to in-plane and out-of-plane rotations.

Combining more than one transformation degrades performance of all networks further, as predicted by a combinatorial model of error (Fig. 6). We next sought to study how the combination of multiple transformations would affect the performance of the networks. For this set of experiments, we use a grey background for all images in order to avoid complex interferences between foreground and background. First, we try combining rotations along the three axes of rotations, YAW, PITCH, and ROLL together (Appendix A.1.1). We find that this combination leads to a degradation of performance for all networks (Fig. 6A) in a range 6%-16.5% compared to the condition where only one axis is rotated at a time. Next we investigate the effect of combining three-axes rotations with scaling (Fig. 6C). We find that this combination of transformation further degrades the performance of all networks, with an accuracy drop in the range 24.5%-78.2% compared to usual poses, larger than the accuracy drop seen for ObjectPose in the range 14.5%-45%. We find that a simple combinatorial model of errors (grey bars in Fig. 6C) recapitulates the accuracy drop well for most of the networks: this model assumes that the probability of the network being correct in the scaled-rotated condition (panel C) is simply the product of the probabilities of being correct in the scaled-only (panel B) and rotated-only (panel A) conditions respectively (see Discussion for implications).

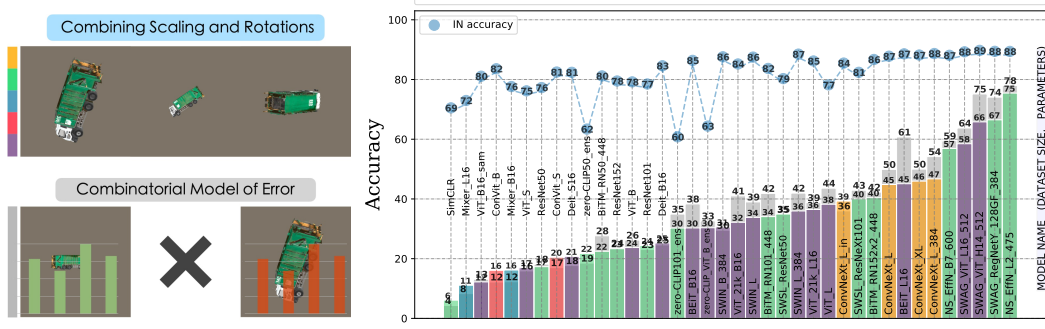
How well do our findings on synthetics datasets transfer to real-world datasets (Fig. 7)? In an attempt to go beyond synthetic datasets, we explore the robustness of our collection of networks to a dataset of real objects filmed from various points of view, the *Common Objects in 3D Dataset* (CO3D) (Reizenstein et al., 2021) (App. A.2). Originally designed for 3D reconstruction and new-view synthesis tasks, this dataset was collected by workers turning around and filming common object from their environment. We sample 1000 images from each of 10 categories common to CO3D and ImageNet, to get a total of about 10,000 images. We then estimate the performance of our collection of networks on these images (Fig. 7). As a point of comparison, we measure the accuracy of networks on images of the same object categories taken from ImageNetV2 (App. A.3), a dataset where objects are mostly presented in their usual canonical view. ImageNetV2 can be seen as a fairer comparison benchmark to CO3D than ImageNet, as networks were not overfitted to the exact statistics of ImageNetV2 (Recht et al., 2019b). We observe an average accuracy drop across networks of 10.4% on ImageNetV2 over ImageNet, and an average accuracy drop of 5.2% on CO3D over ImageNetV2. However, four networks trained on very large datasets perform nearly as well on both



(A) Combining rotations along three axes



(B) Effect of scale on accuracy



(C) Combining three-axes rotations and scale

Figure 6: **Effect of combining multiple transformations on performance.** (A) Combining rotations along the three axes ROLL, PITCH and YAW decreases the accuracy of all networks (colored bars) compared to the single-axis rotation condition (grey bars). (B) Scaling the object size in the image decreases the accuracy severely for most networks (colored bars) compared to the fixed-scaled upright condition (grey bars), but only slightly for the best networks. (C) Combining three-axes rotations and scaling strongly affects the accuracy of all networks (colored bars), with the best network (Noisy Student) at 75% accuracy only in this condition. The grey bars represent a combinatorial model of error which predicts performance degradation well (see text).

datasets: CLIP-RN-101, CLIP-ViT-B/16, Noisy Student EfficientNet-B7, and SWAG-ViT (Fig. 7B). In summary, the variety of object views seen in CO3D seems less problematic for our collection of networks than the views from of our synthetic dataset ObjectPose. This discrepancy could be due to the fact that although the workers turn around the objects in CO3D, they do not necessarily explore all the unusual views that we can explore in our synthetic dataset.

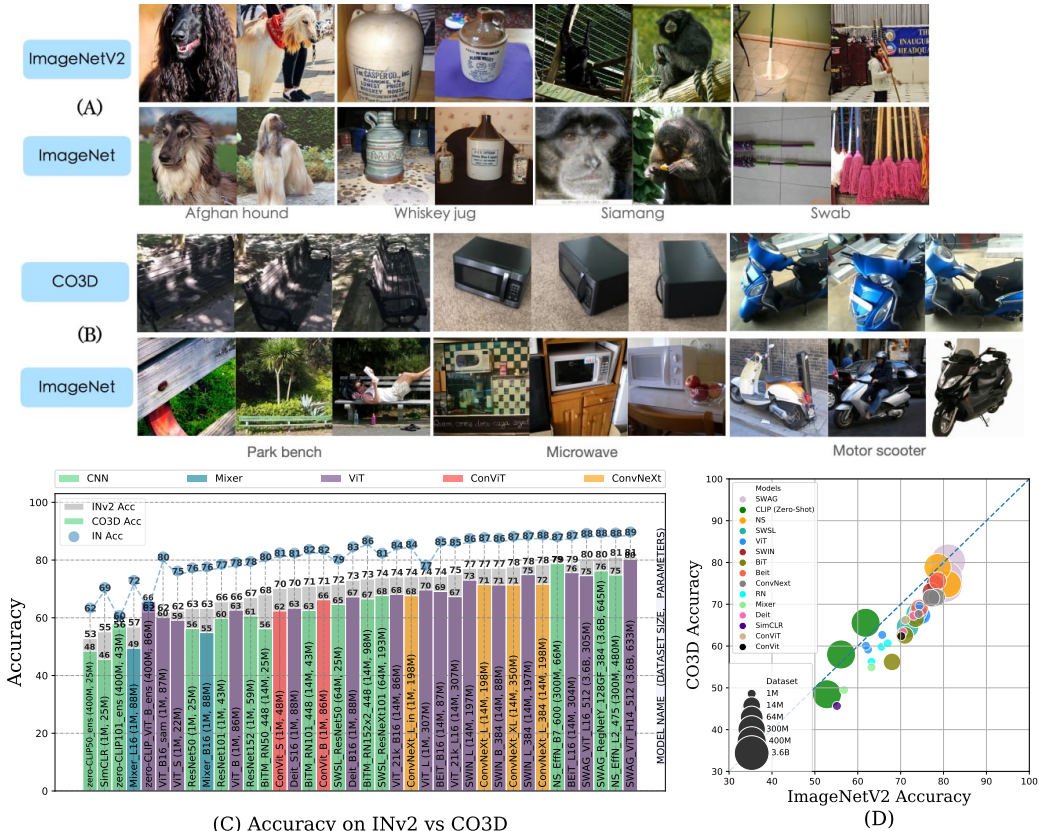


Figure 7: **Going beyond synthetic datasets.** (A) Comparison of images from ImageNet and ImageNetV2, a near-distribution dataset with mostly canonical views. (B) Comparison of images from ImageNet and CO3D, a dataset of objects in unusual views. (C-D) Most networks perform worse on CO3D (colored bars), a dataset exploring various object views, than on ImageNetV2 (grey bars), which mostly presents objects in their usual canonical views (average accuracy drop of 5.2% between the two datasets). ImageNetV2 is a fairer comparison benchmark to CO3D than ImageNet as there was no overfitting it.

4 Discussion

Probing the robustness of deep networks to objects in unusual poses is interesting for multiple reasons. First, this type transformation changes the global structure of the image, which might represent a bigger challenge for deep networks than local image distortions. Second, data-augmentation strategies do not provide an easy fix to the problem of generalization to unusual poses. Indeed, a classical mitigation strategy in deep learning consists in augmenting the dataset with the out-of-distribution case that one would like to become robust to, effectively making that case in-distribution. For most image distortions, this augmentation strategy is easy to implement. But for objects in unusual poses, one would need to collect a very large number of images of objects in unusual poses, which is practically challenging, especially at the scale needed to compete with the best current networks (e.g., Noisy Student is trained on JFT-300M comprising 300 million images). Alternatively, one could synthetically generate such a dataset with 3D models of objects, but this would require a very large database of high-quality 3D models which is currently lacking.

A striking result of our study is that very large networks trained on very large datasets (e.g., Noisy Student trained JFT-300M, SWAG trained on 3.6B Instagram images) are quite robust to unusual poses. However, a careful visual inspection of the errors made by these networks reveal that they do not yet meet the robustness of the human visual system. A thorough comparison to human would be useful to estimate the fraction of the errors that are due to the images themselves not containing enough information about the class (e.g., a jeep seen from the bottom could be any sort of car) vs.

out-of-distribution generalization errors that a human would not fall into (e.g., a cannon seen at a 90° angle is confused by the network with a harp). In future work, we plan to establish this human benchmark on our custom dataset ObjectPose in order to precisely quantify the gap in robustness between humans and networks.

Having the possibility to feed language qualifiers to deep networks is a promising avenue to allow them to adapt to all sorts of out-of-distribution situations. For example in our case, one could indicate to the network to look for an object in an unusual pose. In our experiments with CLIP (Appendix C.2), we do see a slight improvement in performance when prompting the network with textual indications that the object to detect is in an unusual pose (e.g., "an upside-down forklift"). Although promising, the improvement in accuracy we observe remains marginal for this model.

When combining object rotations and scaling, we find that a combinatorial model of error—which assumes that the probability of the network being correct on the combination of transformations is equal to the product of the probabilities of it being correct on each respective transformation—accounts well for the degradation of performance of most networks. It would be interesting to study whether networks’ performance degrade according to this combinatorial model when combining even more transformations, such as translations, texture-removals etc. Indeed, an implication of this combinatorial model of error is that networks should be brittle in the face of a large combination of transformations, as each factor of variation adds its own source for potential errors.

It is an open question how the human visual system builds robustness to unusual poses. When performing mental rotation, a task consisting in comparing two 3D shapes in different orientations, human subjects take a time to respond that scales linearly with the angle of rotation between the two shapes (Shepard and Metzler, 1971). A similar phenomenon happens when recognizing every-day-life objects in unusual orientations (Jolicoeur, 1985): the recognition time is again linear with the angle of the object with respect to its upright pose. These observations are striking as they suggest that different mechanisms take place in the brain compared to feed-forward deep networks, where the processing time is fixed and does not depend on the complexity of the input image. We hypothesize that recurrent mechanisms may play a key role in recognizing objects in unusual poses in the brain, as there is mounting evidence that such mechanisms are critical for recognizing images that are challenging to deep networks (Kar et al., 2019; Bonnen et al., 2021).

Acknowledgements and Author Contributions

We thank Alcorn et al. (2019) and Geirhos et al. (2021) for making their codebases publicly available. We thank Robert Geirhos, Michael Alcorn, Anh Nguyen, and the OOD group at Meta AI (led by Pascal Vincent) for their kind feedback and suggestions to improve this work. We also thank Google for providing GCP credits for the project. Author contributions: analyses and visualizations performed by A.A.; conceptualization, interpretation and writing by A.A. and S.D.

References

- Michael A Alcorn, Qi Li, Zhitao Gong, Chengfei Wang, Long Mai, Wei-Shinn Ku, and Anh Nguyen. Strike (with) a pose: Neural networks are easily fooled by strange poses of familiar objects. In *Proceedings of the IEEE/CVF Conference on Computer Vision and Pattern Recognition*, pages 4845–4854, 2019.
- Hangbo Bao, Li Dong, and Furu Wei. Beit: Bert pre-training of image transformers. *arXiv preprint arXiv:2106.08254*, 2021.
- Tyler Bonnen, Daniel L. K. Yamins, and Anthony D. Wagner. When the ventral visual stream is not enough: A deep learning account of medial temporal lobe involvement in perception. *Neuron*, 109(17):2755–2766.e6, September 2021. ISSN 0896-6273. doi: 10.1016/j.neuron.2021.06.018. URL <https://www.sciencedirect.com/science/article/pii/S0896627321004591>.
- Ting Chen, Simon Kornblith, Mohammad Norouzi, and Geoffrey Hinton. A simple framework for contrastive learning of visual representations. In *International conference on machine learning*, pages 1597–1607. PMLR, 2020a.

- Ting Chen, Simon Kornblith, Kevin Swersky, Mohammad Norouzi, and Geoffrey E Hinton. Big self-supervised models are strong semi-supervised learners. *Advances in neural information processing systems*, 33:22243–22255, 2020b.
- Xiangning Chen, Cho-Jui Hsieh, and Boqing Gong. When vision transformers outperform resnets without pre-training or strong data augmentations. *arXiv preprint arXiv:2106.01548*, 2021.
- Ekin D Cubuk, Barret Zoph, Jonathon Shlens, and Quoc V Le. Randaugment: Practical automated data augmentation with a reduced search space. In *Proceedings of the IEEE/CVF conference on computer vision and pattern recognition workshops*, pages 702–703, 2020.
- Stéphane d’Ascoli, Hugo Touvron, Matthew Leavitt, Ari Morcos, Giulio Biroli, and Levent Sagun. Convit: Improving vision transformers with soft convolutional inductive biases. *arXiv preprint arXiv:2103.10697*, 2021.
- Jacob Devlin, Ming-Wei Chang, Kenton Lee, and Kristina Toutanova. Bert: Pre-training of deep bidirectional transformers for language understanding. *arXiv preprint arXiv:1810.04805*, 2018.
- Samuel Dodge and Lina Karam. A study and comparison of human and deep learning recognition performance under visual distortions. In *2017 26th international conference on computer communication and networks (ICCCN)*, pages 1–7. IEEE, 2017.
- Alexey Dosovitskiy, Lucas Beyer, Alexander Kolesnikov, Dirk Weissenborn, Xiaohua Zhai, Thomas Unterthiner, Mostafa Dehghani, Matthias Minderer, Georg Heigold, Sylvain Gelly, et al. An image is worth 16x16 words: Transformers for image recognition at scale. *arXiv preprint arXiv:2010.11929*, 2020.
- Pierre Foret, Ariel Kleiner, Hossein Mobahi, and Behnam Neyshabur. Sharpness-aware minimization for efficiently improving generalization. *arXiv preprint arXiv:2010.01412*, 2020.
- Robert Geirhos, Carlos RM Temme, Jonas Rauber, Heiko H Schütt, Matthias Bethge, and Felix A Wichmann. Generalisation in humans and deep neural networks. *Advances in neural information processing systems*, 31, 2018.
- Robert Geirhos, Kantharaju Narayanappa, Benjamin Mitzkus, Tizian Thieringer, Matthias Bethge, Felix A Wichmann, and Wieland Brendel. Partial success in closing the gap between human and machine vision. *arXiv preprint arXiv:2106.07411*, 2021.
- Kaiming He, Xiangyu Zhang, Shaoqing Ren, and Jian Sun. Deep residual learning for image recognition. In *Proceedings of the IEEE conference on computer vision and pattern recognition*, pages 770–778, 2016.
- Dan Hendrycks and Thomas Dietterich. Benchmarking neural network robustness to common corruptions and perturbations. *arXiv preprint arXiv:1903.12261*, 2019.
- Dan Hendrycks, Steven Basart, Norman Mu, Saurav Kadavath, Frank Wang, Evan Dorundo, Rahul Desai, Tyler Zhu, Samyak Parajuli, Mike Guo, Dawn Song, Jacob Steinhardt, and Justin Gilmer. The many faces of robustness: A critical analysis of out-of-distribution generalization. *ICCV*, 2021a.
- Dan Hendrycks, Kevin Zhao, Steven Basart, Jacob Steinhardt, and Dawn Song. Natural adversarial examples. In *Proceedings of the IEEE/CVF Conference on Computer Vision and Pattern Recognition*, pages 15262–15271, 2021b.
- Geoffrey Hinton, Oriol Vinyals, Jeff Dean, et al. Distilling the knowledge in a neural network. *arXiv preprint arXiv:1503.02531*, 2(7), 2015.
- Pierre Jolicoeur. The time to name disoriented natural objects. *Memory & Cognition*, 13(4):289–303, 1985. ISSN 1532-5946. doi: 10.3758/BF03202498. Place: US Publisher: Psychonomic Society.
- Kohitij Kar, Jonas Kubilius, Kailyn Schmidt, Elias B. Issa, and James J. DiCarlo. Evidence that recurrent circuits are critical to the ventral stream’s execution of core object recognition behavior. *Nature Neuroscience*, 22(6):974–983, June 2019. ISSN 1546-1726. doi: 10.1038/s41593-019-0392-5. URL <https://www.nature.com/articles/s41593-019-0392-5>. Number: 6 Publisher: Nature Publishing Group.

- Alexander Kolesnikov, Lucas Beyer, Xiaohua Zhai, Joan Puigcerver, Jessica Yung, Sylvain Gelly, and Neil Houlsby. Big transfer (bit): General visual representation learning. In *European conference on computer vision*, pages 491–507. Springer, 2020.
- Ze Liu, Yutong Lin, Yue Cao, Han Hu, Yixuan Wei, Zheng Zhang, Stephen Lin, and Baining Guo. Swin transformer: Hierarchical vision transformer using shifted windows. In *Proceedings of the IEEE/CVF International Conference on Computer Vision*, pages 10012–10022, 2021.
- Zhuang Liu, Hanzi Mao, Chao-Yuan Wu, Christoph Feichtenhofer, Trevor Darrell, and Saining Xie. A convnet for the 2020s. *arXiv preprint arXiv:2201.03545*, 2022.
- Spandan Madan, Tomotake Sasaki, Tzu-Mao Li, Xavier Boix, and Hanspeter Pfister. Small in-distribution changes in 3D perspective and lighting fool both CNNs and Transformers. *arXiv*, 2021.
- John P Miller, Rohan Taori, Aditi Raghunathan, Shiori Sagawa, Pang Wei Koh, Vaishaal Shankar, Percy Liang, Yair Carmon, and Ludwig Schmidt. Accuracy on the line: on the strong correlation between out-of-distribution and in-distribution generalization. In *International Conference on Machine Learning*, pages 7721–7735. PMLR, 2021.
- Hieu Pham, Zihang Dai, Qizhe Xie, and Quoc V Le. Meta pseudo labels. In *Proceedings of the IEEE/CVF Conference on Computer Vision and Pattern Recognition*, pages 11557–11568, 2021.
- Alec Radford, Jong Wook Kim, Chris Hallacy, Aditya Ramesh, Gabriel Goh, Sandhini Agarwal, Girish Sastry, Amanda Askell, Pamela Mishkin, Jack Clark, et al. Learning transferable visual models from natural language supervision. In *International Conference on Machine Learning*, pages 8748–8763. PMLR, 2021.
- Benjamin Recht, Rebecca Roelofs, Ludwig Schmidt, and Vaishaal Shankar. Do imagenet classifiers generalize to imagenet? In *International Conference on Machine Learning*, pages 5389–5400. PMLR, 2019a.
- Benjamin Recht, Rebecca Roelofs, Ludwig Schmidt, and Vaishaal Shankar. Do ImageNet Classifiers Generalize to ImageNet? In *International Conference on Machine Learning*, 2019b.
- Jeremy Reizenstein, Roman Shapovalov, Philipp Henzler, Luca Sbordone, Patrick Labatut, and David Novotny. Common objects in 3d: Large-scale learning and evaluation of real-life 3d category reconstruction. In *Proceedings of the IEEE/CVF International Conference on Computer Vision*, pages 10901–10911, 2021.
- Olga Russakovsky, Jia Deng, Hao Su, Jonathan Krause, Sanjeev Satheesh, Sean Ma, Zhiheng Huang, Andrej Karpathy, Aditya Khosla, Michael Bernstein, et al. Imagenet large scale visual recognition challenge. *International journal of computer vision*, 115(3):211–252, 2015.
- Vaishaal Shankar, Achal Dave, Rebecca Roelofs, Deva Ramanan, Benjamin Recht, and Ludwig Schmidt. Do image classifiers generalize across time? In *Proceedings of the IEEE/CVF International Conference on Computer Vision*, pages 9661–9669, 2021.
- Roger N. Shepard and Jacqueline Metzler. Mental rotation of three-dimensional objects. *Science*, 171(3972):701–703, 1971. ISSN 1095-9203. doi: 10.1126/science.171.3972.701. Place: US Publisher: American Assn for the Advancement of Science.
- Mannat Singh, Laura Gustafson, Aaron Adcock, Vinicius de Freitas Reis, Bugra Gedik, Raj Prateek Kosaraju, Dhruv Mahajan, Ross Girshick, Piotr Dollár, and Laurens van der Maaten. Revisiting weakly supervised pre-training of visual perception models. In *Proceedings of the IEEE/CVF Conference on Computer Vision and Pattern Recognition*, pages 804–814, 2022.
- Christian Szegedy, Vincent Vanhoucke, Sergey Ioffe, Jon Shlens, and Zbigniew Wojna. Rethinking the inception architecture for computer vision. In *Proceedings of the IEEE conference on computer vision and pattern recognition*, pages 2818–2826, 2016.
- Rohan Taori, Achal Dave, Vaishaal Shankar, Nicholas Carlini, Benjamin Recht, and Ludwig Schmidt. Measuring robustness to natural distribution shifts in image classification. *Advances in Neural Information Processing Systems*, 33:18583–18599, 2020.

- Ilya O Tolstikhin, Neil Houlsby, Alexander Kolesnikov, Lucas Beyer, Xiaohua Zhai, Thomas Unterthiner, Jessica Yung, Andreas Steiner, Daniel Keysers, Jakob Uszkoreit, et al. Mlp-mixer: An all-mlp architecture for vision. *Advances in Neural Information Processing Systems*, 34, 2021.
- Hugo Touvron, Matthieu Cord, Matthijs Douze, Francisco Massa, Alexandre Sablayrolles, and Hervé Jégou. Training data-efficient image transformers & distillation through attention. In *International Conference on Machine Learning*, pages 10347–10357. PMLR, 2021.
- Haohan Wang, Songwei Ge, Zachary Lipton, and Eric P Xing. Learning robust global representations by penalizing local predictive power. In *Advances in Neural Information Processing Systems*, pages 10506–10518, 2019.
- Qizhe Xie, Minh-Thang Luong, Eduard Hovy, and Quoc V Le. Self-training with noisy student improves imagenet classification. In *Proceedings of the IEEE/CVF conference on computer vision and pattern recognition*, pages 10687–10698, 2020.
- Lu Yuan, Dongdong Chen, Yi-Ling Chen, Noel Codella, Xiyang Dai, Jianfeng Gao, Houdong Hu, Xuedong Huang, Boxin Li, Chunyuan Li, et al. Florence: A new foundation model for computer vision. *arXiv preprint arXiv:2111.11432*, 2021.

Appendix

A Datasets

In this section, we describe in detail the three datasets we use in our experiments: (1) our custom dataset ObjectPose, which measures the robustness of networks’ to unusual object poses, (2) our adaptation of the CO3D dataset (Reizenstein et al., 2021), which measures the generalization capability of networks’ on various natural poses, (3) ImageNetV2 (Recht et al., 2019a), which measures the generalization capability of networks’ to a similar distribution than ImageNet while preventing overfitting effects to ImageNet’s exact statistics.

A.1 ObjectPose Dataset

To measure the robustness of the models to unusual object poses, we generated a synthetic dataset of objects in unusual poses, ObjectPose. The dataset contains around 27,540 images of objects in unusual poses. It covers 17 of the 1000 ImageNet ILSVRC-2012 (Russakovsky et al., 2015) image classification task classes. Each image in the dataset contains only one ImageNet object centered in the image. The dataset was created by rendering high-quality 3D objects on top of a background image following the pipeline introduced in (Alcorn et al., 2019) and building on their codebase made available online. The images are generated by rotating the 3D object along one axis to put it in an unusual pose and then rendering the object on top of the background. The 17 object categories in ObjectPose are ‘airliner’, ‘barber chair’, ‘cannon’, ‘fire engine’, ‘folding chair’, ‘forklift’, ‘garbage truck’, ‘hammerhead shark’, ‘jeep’, ‘mountain bike’, ‘park bench’, ‘rocking chair’, ‘shopping cart’, ‘table lamp/ lampshade’, ‘tank’, ‘tractor’, and ‘wheel barrow’. To focus more on the effect of the poses we consider both ‘table lamp’ and ‘lampshade’ as correct labels for table lamp images in ObjectPose. The dataset is designed carefully so that the images are easy to classify when the object is upright.

3D objects: We picked the 3D objects very carefully so they all have high quality. To make sure that the 2D images generated from the 3D objects have high quality and look realistic at the same time, we first manually excluded all the 3D objects that don’t give realistic 2D images, then we run the evaluation experiment explained in section (A.1.2) to make sure that the images have sufficient quality. We excluded all the 3D objects that do not pass this evaluation. Section (A.1.4) provides more details about the 3D objects we used.

Background images: To increase the diversity of the dataset we used three different backgrounds with each object. Each time, we render the 3D objects on top of one of these backgrounds. Two of the backgrounds are natural background images chosen manually from the internet. We chose each background image carefully so that it matches the object and does not contain any of the ImageNet ILSVRC-2012 dataset objects. Following (Alcorn et al., 2019), we chose the third background to be grey background with all its RGB pixel values equal to (0.485, 0.456, 0.406). These values correspond to the average pixel color of ImageNet images.

A.1.1 ObjectPose Dataset Generation

The ObjectPose dataset was generated using a 3D renderer following the pipeline introduced in (Alcorn et al., 2019). For each 3D object we choose three rotation axes. These axes are orthogonal to the 3D object and defined relative to it. For each of the three axes, we create 180 images that cover the 360 rotation degrees by rotating the 3D object along this axis.

Rotating the object is done by using three 3x3 rotation matrices R_r , R_y , R_p . Each matrix is defined by one rotation angle ϕ_y , ϕ_r , or ϕ_p respectively. These matrices correspond to the rotation around the *YAW*, *ROLL*, and *PITCH* axes respectively. These are the axes orthogonal to the 3D object as shown in Fig. 8. To generate the images, first, we manually choose the initial rotation angles ϕ_y° , ϕ_r° , and ϕ_p° that place the object in a usual pose, then each time we increase the rotation angle by two degrees along one axis and render the 3D object on top of the background to get a 2D image. In order to better blend the object in its initial pose, we also perform 3D translation. We adjust the three

translation parameters x , y , and z manually for each 3D object. We choose x and y to be near zero so that the object is centered and reasonably placed in the 2D image. The z parameter controls how close the object is to the camera. We set the value of z manually for each object.

Let R be a 3D renderer that takes as input a set of parameters $\Theta = \{\phi_y, \phi_r, \phi_p, x, y, z, Obj, C, BG, L\}$ and outputs 2D image following the pipeline in (Alcorn et al., 2019) defined by equation (1).

$$I = R(\phi_y, \phi_r, \phi_p, x, y, z, Obj, L, BG) \quad (1)$$

Where $I \in \mathbb{R}^{H \times W \times 3}$ is the 2D image. H and W represent the dimensions of the image. Here Obj , BG , L are the 3D object, the background image, and the lighting parameters respectively. The lighting parameter L is used to control the ambient light and the directional light in the image. We set the ambient light intensity manually for each object separately, while keeping the directional light oriented at $(0.3, 1.0, 1.0)$ with its intensity fixed at 0.9 according to the settings defined in (Alcorn et al., 2019).

For each of the 17 3D objects there are 180×9 images (9 because we have three backgrounds and three rotation axes). This gives a balanced dataset with a total of 27,540 images. In order to discard usual poses, we then exclude all images with an angle smaller than 10° with respect to the upright pose, keeping only the range $[11^\circ, 349^\circ]$. All the images have a size of 500×500 pixels. Samples from the dataset are shown in Fig. 12 in the appendix.

Choosing the rotation axes: After placing the object in the initial position (the first column in Fig. 8), we choose one of the *YAW*, *ROLL*, or *PITCH* axes to rotate the object along it. When choosing the rotation axis, we consider only the axes that result in unusual poses. For example, rotating the truck in Fig. 8 around the *YAW* axis does not result in the unusual poses we want, that is why we do not rotate the truck around the *YAW* axis for this specific object. The truck object is rotated along the *ROLL* axis (with two different initialization), and along the *PITCH* axis. This gives us three different rotations for this object (Fig. 8). We follow the same process for generating the images from all the 3D objects. The kind of rotation we follow to generate the dataset is considered as out-of-plane rotation.

In addition to the main ObjectPose dataset, we created five additional datasets. Each one measures the robustness of networks to different conditions:

Image-rotation dataset: Here we take one 2D image from the ObjectPose dataset with the object on the manually chosen usual pose, then we generate 180 images from the image by rotating it by 360° with a 2° step. To avoid border-cropping effects while rotating the image, we filled the image corners with grey color using a circular crop. Fig. 9 shows how images are generated.

In-plane rotation vs out-of-plane rotation: Another kind of rotation that we are testing is the in-plane rotation. The in-plane rotation is similar to the image rotation by the fact that for both of them the object is rotated around the same axis—the axis orthogonal to the screen. The difference is that for in-plane rotations, we fix the background in its upright position, in contrast to the 2D-image rotations. Comparing the out-of-plane rotation (ObjectPose) to the in-plane rotation, we notice that the background is fixed for both, while the rotation axis is different. For the out-of-plane case, the rotation axis is orthogonal to the 3D object, but for the in-plane rotation case, the rotation axis is orthogonal to the 2D image (the screen). Fig. 9 describes the in-plane rotation visually.

ObjectScale dataset: To study the effect of reducing the object scale, we created a dataset of images showing objects at different scales. Starting from the scale used for ObjectPose, we scale down the object by increasing the value of the z parameter of the 3D renderer. The object is scaled down until its resolution approaches the limit of what can be recognized by (our) eye. Using two different initializations, 35 images were created for each object on average. The dataset contains 593 images in total. To avoid any mismatch between the object size and background we used grey background images only. See Fig. 10 for samples from the dataset.

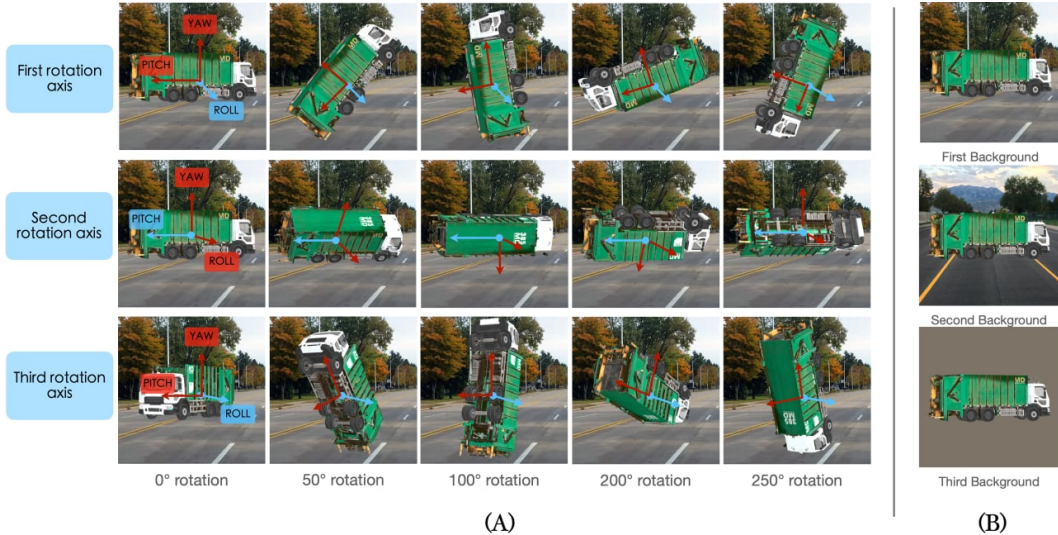


Figure 8: **ObjectPose dataset generation.** (A) The figure shows how the object is rotated around the three different axes. First, we manually align the object to be in a natural pose with the background (*First Column*). This defines the relative zero rotation angle with respect to the initial position. *Rows*: Each row shows the rotation of the object along a different axis. The rotation axes are orthogonal to the 3D object as shown with the arrows. The blue arrow corresponds to the rotation axis in each row. (B) Three different backgrounds used with the truck object, two are natural images, and the third one is grey.

Three-axes rotation dataset: This time we rotate the object randomly along the axes *ROLL*, *YAW*, and *PITCH* at the same time. For each 3D object, 180 images were created by sampling the three rotation angles randomly each time. For fair comparison, only grey background is used for creating this dataset. Fig. 10 shows some samples from the dataset.

Combining scale and rotation dataset: The dataset is created by combining two types of transformations, three-axes rotation and scaling. The rotation angles are samples randomly from the range (0, 360). For fair comparison to using single transformations, the scale is sampled randomly from the same range used to create ObjectScale dataset. For each object, 180 images with grey background were created. Samples from the dataset are shown in Fig. 10.

Background Rotation dataset: Using two different initializations the object is fixed and 180 images are created for each initialization by rotating the background by 360° with a step of 2° . The image corners are filled with grey color. See Fig. 10 for samples from the dataset.

A.1.2 ObjectPose Dataset Evaluation

Since we do not want anything else than the object pose to affect the model decision, we performed a simple experiment to evaluate the ObjectPose dataset quality. The experiment evaluates the dataset by testing the models on a subset of images with the objects in usual poses (upright). These are the images from ObjectPose with the object rotated by -10 to 10 degrees only. We call this dataset ObjectPose +/-10. It consists of 1,683 images in total. We consider ObjectPose +/-10 as usual-pose images and ObjectPose as unusual-pose images.

While we are generating the ObjectPose dataset, we excluded all the 3D objects with a ResNet50 (He et al., 2016) top1 accuracy of less than 90% on ObjectPose +/-10. Among approximately 30 3D objects evaluated, we selected 17 of them for the ObjectPose dataset. Following (Hendrycks et al., 2021b), we chose ResNet50 because it has a moderate ImageNet top1 accuracy of 76.1%.

The objects are very easy to detect in usual poses: After generating the ObjectPose dataset, we tested all the 38 models on ObjectPose +/-10. The results are shown in Fig. 11. We see from the results that on ObjectPose +/-10, ResNet-50 achieves 93% average accuracy, which is higher than ResNet-50 top1 accuracy on ImageNet (76.1%). Clearly, we see that most of the models obtain

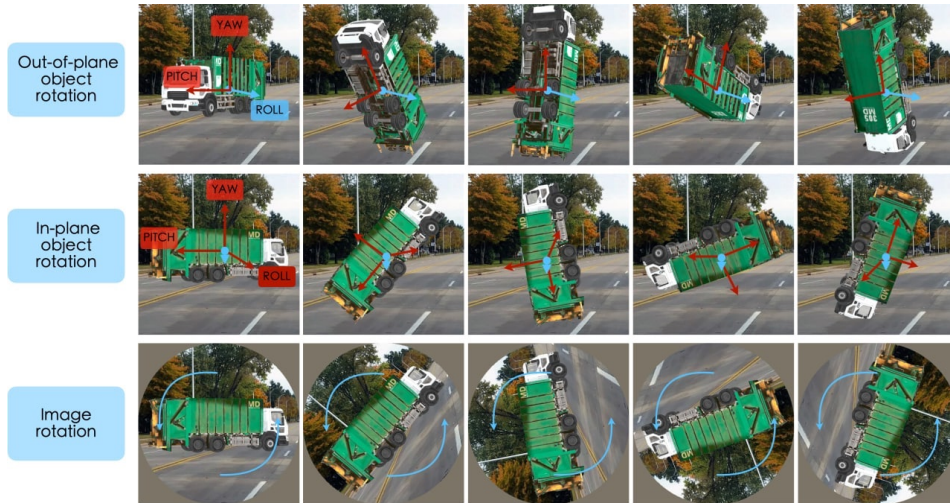
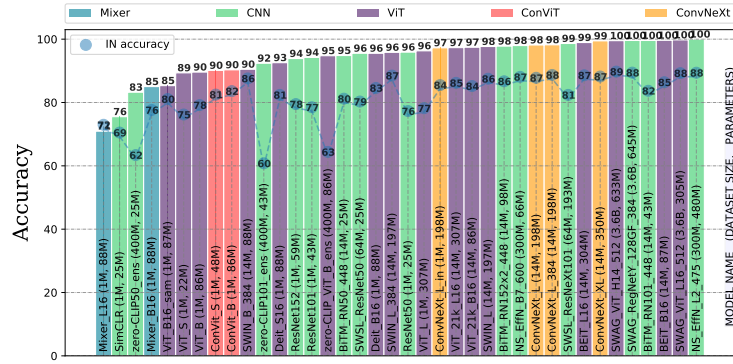


Figure 9: **Out-of-plane vs In-plane vs 2D image-rotation**: For out-of-plane rotations (ObjectPose), the rotation axis is orthogonal to the object. The **in-plane rotation** is similar to rotating the 2D image (image rotation) while fixing the background, such that we always see the same view of the object. For the **image rotation**, we rotate the 2D image itself, and the corners are filled with grey to avoid border-cropping effects.



Figure 10: Different datasets to test different kinds of transformations.

accuracy higher than 80%. All the models perform on ObjectPose +-10 better than on ImageNet test dataset. This indicates that the method we follow to generate ObjectPose dataset gives high-quality images that look realistic for the models.



Result on ObjectPose +10° (Usual Poses)

Figure 11: The performance on ObjectPose +10. Most of the models can detect the objects in the usual poses. Note that CLIP models are trained on the WebImageText dataset and tested here without fine-tuning on ImageNet.

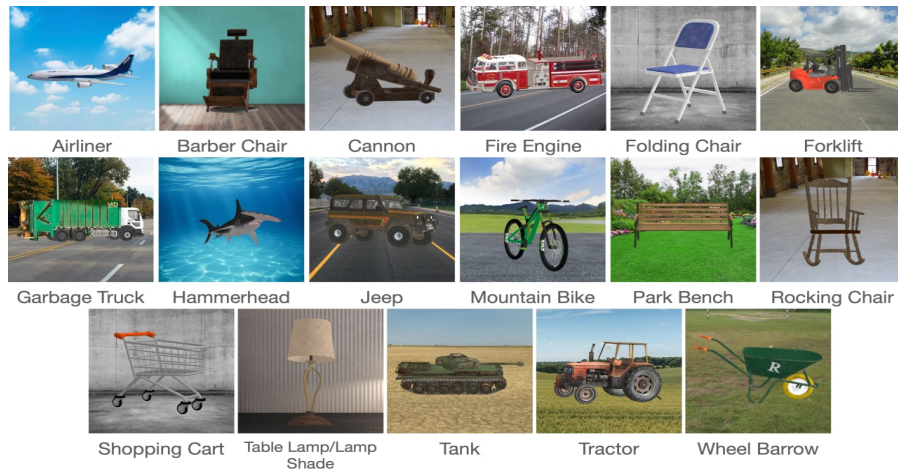


Figure 12: Presentation of the 17 3D objects composing ObjectPose. These objects were carefully selected from <https://sketchfab.com/> for their visual quality as well as the ability of a ResNet-50 to correctly classify them in their upright pose. They were then rendered on a background image which we selected to correspond semantically to the object (e.g., a jeep is on a road).

A.1.3 Background Images for ObjectPose Dataset

The background images used for ObjectPose dataset were downloaded from the internet. Some of the background images are shared between more than one 3D object. In total, we use 24 different background images. Each background was chosen to logically match the object (i.e. a road background image for the Garbage Truck object). Fig. 12 shows some sample images from ObjectPose dataset with different backgrounds.

A.1.4 The 3D Objects

All the 17 3D objects we selected were downloaded from <https://sketchfab.com>. All the objects are in *.obj* format.

- Barber chair: [link](#)
- Shopping cart: [link](#)
- Rocking chair: [link](#)
- Mountain Bike: (edited: the texture was changed) [link](#)

- Forklift: [link](#)
- Wheel barrow: [link](#)
- Folding Chair: [link](#)
- Fire engine: [link](#)
- Garbage Truck: [link](#)
- Tractor: [link](#)
- Tank: [link](#)
- Jeep (edited: some of the object parts were removed and some parts were scaled): [link](#)
- Cannon: [link](#)
- Hammerhead Shark: [link](#)
- Park Bench: [link](#)
- Table Lamp: [link](#)
- Airliner: [link](#)

A.2 CO3D Dataset

The Common Objects in 3D (CO3D) dataset (Reizenstein et al., 2021) was originally designed for 3D reconstruction and new-view synthesis tasks. The dataset contains real-world multi-view videos of 50 common object categories. The videos were collected by workers from their own environment using their own devices. The dataset shares some of its 50 object categories with the 1000-classes ImageNet ILSVRC-2012 dataset (Russakovsky et al., 2015). In our experiments, we use a subset from CO3D videos with the following 10 object categories: ‘bench’, ‘motorscooter’, ‘toilet’, ‘toaster’, ‘parking meter’, ‘broccoli’, ‘microwave’, ‘banana’, ‘hotdog’, and ‘bicycle’. We sampled 1000 images from videos of each of these 10 categories to get a total of about 10,000 images. In the rest of the paper, we will refer to this subset of 10,000 images as CO3D.

Selecting Subset From CO3D: For each category, the CO3D dataset provides a set of folders, each one containing a set of images for one object. These images are sampled from a video taken for the object by walking in a complete circle around the object. In this way, we get images from different views and poses. In all the images, there is only one object centered in the image. Each category has a different number of folders available. When selecting a subset from CO3D, we sampled k images from each folder so that the total number of images we have for the category is 1000 images (ie. we sample $1000/k$ images from each folder). When reviewing CO3D dataset, we found that for some folders, the kinds of objects in CO3D don’t always perfectly match the kind of objects in ImageNet. As an example, the bench category in CO3D dataset includes images of objects such as park benches, sofas, and other kinds of benches, while ImageNet includes images of park benches only. To solve this, we manually reviewed the images of the 10 object categories in CO3D and compared them to the images of the same categories in the ImageNet validation dataset, and then we manually excluded all the folders with images that don’t match ImageNet. After filtering the dataset, we sampled 1000 images from each category. This gives us a balanced dataset of 10 classes and 10,000 images in total. Fig. 7 shows samples from the dataset.

A.3 ImageNetV2 Dataset

ImageNetV2 was introduced in (Recht et al., 2019a) as a new testset to measure the generalization of ImageNet classifiers. The dataset was collected from the internet following the same dataset creation process as the original ImageNet dataset (Russakovsky et al., 2015). It mimics ImageNet by the fact that both of them are clean internet images collected from the Flickr hosting service and both of them contain images uploaded to the internet during the same period of time. The dataset helps in measuring the performance of networks on a distribution as close as possible to the training distribution (near-distribution), while avoiding overfitting effects to ImageNet’s exact statistics. It consists of 10,009 images with fewer examples per class than ImageNet. Fig. 7 shows some examples sampled randomly from the same classes from both ImageNet and ImageNetV2. The figure shows how the two datasets are similar. In our experiments, we use the "Matched Frequency" version of ImageNetV2 dataset.

B Deep Networks details

B.1 Datasets and Training Objectives

The models were trained on datasets with different sizes ranging from 1 million to 3.6 billions images. Among the models we use, Noisy Student EfficientNet (Xie et al., 2020) (300M images) and SWAG (Singh et al., 2022) (3.6B images) are the only models pretrained on extremely large dataset and fine-tuned on ImageNet. Although CLIP (Radford et al., 2021) is also pretrained on a very large dataset (400M image-text pairs), it is not fine-tuned on ImageNet. We also chose models trained under different objectives, including:

- Supervised learning, including convolutional architectures, such as (He et al., 2016) (Xie et al., 2020) (Liu et al., 2022) (Kolesnikov et al., 2020), Vision Transformers, such as (Dosovitskiy et al., 2020) (Chen et al., 2021)(Bao et al., 2021) (Touvron et al., 2021) (Liu et al., 2021), (Liu et al., 2022), and MLP-mixer(Tolstikhin et al., 2021),
- Self-supervised learning, such as SimCLR (Chen et al., 2020a), and BEiT (Bao et al., 2021),
- Semi-weakly supervised learning, such as SWSL-ResNet50 and SWSL-ResNeXt101 (Chen et al., 2020b), and weakly supervised learning, such as SWAG (Singh et al., 2022),
- Text supervision, such as CLIP (Radford et al., 2021).

We also included models trained using special optimizers such as the ViT-B16-SAM model (Chen et al., 2021), a vision transformer trained with the recently proposed optimizer SAM (Foret et al., 2020), which is designed to improve generalization and robustness.

B.2 Model descriptions

In this section, we describe in detail the networks tested in this study. Table (1) shows the full list of models.

CLIP: CLIP was introduced in (Radford et al., 2021) as a model trained using a unique text supervision objective that works as an alternative to the (image, label) supervision. The model is pretrained using an image-caption matching task where we pass the image and its caption to the model. The task is simply to predict which caption matches which image. The model is supervised by the image caption text, then it is asked to maximize the similarity between the image representation and the caption representation of the paired inputs and to minimize the similarity between the representations of the unpaired inputs using a contrastive loss. The model consists of an image encoder that processes the image and outputs the image representation, and a text encoder that processes the text and outputs the text representation. The model is pretrained on a dataset of 400 million (image, caption) pairs. **textbfZero-shot prediction:** After pretraining the model we can use it for image classification without funetuning on any dataset. This is called zero-shot prediction. The way CLIP is trained makes it easy to perform zero-shot prediction on any image classification dataset. To classify an image for a k -classes classification task, we get the image representation from the pretrained image encoder. We add the name of each of the k classes to a sentence (prompt) and pass all the k sentences to the pretrained text encoder to get the representation of each one of them. Then we compute the cosine similarity between the image representation and all the sentence (prompt) representations. The predicted class is the one associated with the input sentence with the highest similarity to the image. The paper proposed ensembling the predictions over different input sentences to improve the performance. This is done by averaging the representations of more than one text input. In our experiments, we ensemble over 80 input prompts proposed by the authors for ImageNet. We use three zero-shot CLIP models, CLIP-ResNet-50, CLIP-ResNet-101, and CLIP-ViT-B/16.

Standard Vision Transformer: We include six standard Vision Transformers (ViTs) (Dosovitskiy et al., 2020), four of them (ViT-S/16, ViT-B/16, ViT-B16-SAM/16, ViT-L16) were pretrained on ImageNet with input size 224x224. The ViT-B16-SAM/16 model was pretrained using SAM optimizer introduced in (Foret et al., 2020). The last two models are ViT-21k-B/16, and ViT-21k-L/16 pretrained on ImageNet-21k and fine-tuned on ImageNet with the input size of 384x384.

BEiT: The model is a Vision Transformer trained using a self-supervised training method introduced with the model (Bao et al., 2021) known as Masked Image Modeling (MIM). MIM is inspired by the Masked Language Modeling (MLM) task used for training BERT (Devlin et al., 2018) text transformer. BEiT outperforms standard ViT even when using a smaller pretraining dataset. In our experiments we use two BEiT models (BEiT-B/16 and BEiT-L/16). Both of them were pretrained with the self-supervised MIM task on ImageNet22k and fine-tuned on ImageNet.

ConvNext: We also use four ConvNeXt (Liu et al., 2022) models. ConvNeXT was introduced recently as a pure convolutional architecture that competes with the ViT. The convolutional layers of ConvNeXt are designed carefully by choosing a good collection of architecture hyperparameters after running many experiments. The model is trained by following techniques used to train ViTs that were proved to improve the performance of ConvNeXt also.

ConViT: We also use two ConViT models (ConViT-B and ConViT-L)(d’Ascoli et al., 2021). ConViT replaces some of the ViT self-attention layers with a new kind of attention layer called gated positional self-attention (GPSA) layers introduced with the model.

DeiT: We also use two Data-efficient Vision Transformers (DeiT) (Touvron et al., 2021). DeiT was introduced to reduce the need for large pretraining dataset for Vision Transformers. The model relies on a teacher-student knowledge distillation (Hinton et al., 2015) strategy designed for transformers. It can achieve the performance of ViTs with much less data (ImageNet only) while having the same number of parameters. In our experiments, we use DeiT-B/16 and DeiT-S/16.

SWIN Transformer: We also use three SWIN transformers (SWIN-L-384, SWIN-L, and SWIN-B-384). SWIN transformer (Liu et al., 2021) is a hierarchical Vision Transformer that replaces the self-attention layer of the original vision transformer with a Shifted Window Self-attention layer (SWSA). The SWSA layer partitions the image into windows and computes the self-attention locally inside each window. This operation results in reducing the attention layer computational time to be linear to the input size instead of quadratic, while improving the performance over the original ViT.

SimCLR: We use one SimCLR model (Chen et al., 2020a) with ResNet50 backbone. The backbone was trained using a self-supervised contrastive loss without fine-tuning on ImageNet. A linear classifier was trained on top of the backbone architecture to perform classification.

ResNet: We use three ResNets (He et al., 2016) trained on ImageNet. These are ResNet50, ResNet101, and ResNet152.

BiT: Big Transfer was introduced in (Kolesnikov et al., 2020) as a recipe for transfer learning from a large dataset to the target dataset. We use three medium Big Transfer models pretrained on ImageNet21k dataset and fine-tuned on ImageNet. Namely, these are the models BiTM-ResNetv2-50x1, BiTM-ResNetv2-101x1, and BiTM-ResNetv2-152x1.

SWSL: We use two Semi-weakly supervised models (Chen et al., 2020b) (SWSL-ResNeXt101, and SWSL-ResNeXt101-32x16d). The models were pretrained on 64M images extracted from a larger dataset of 940 million using a teacher model. The labels for the 64M images are predicted by the teacher models. The teacher model is a ResNet-101-32x48 pretrained on ImageNet. The models are then fine-tuned on ImageNet

Noisy Student: We use two EfficientNets pretrained using the Noisy Student paradigm introduced in (Xie et al., 2020). The models are trained on a combination of a noisily labeled JFT-300M dataset and ImageNet dataset. The two models are Noisy Student EfficientNet-L2 with an input size of 475x475, and Noisy Student EfficientNet-B7 with an input size of 600x600. These models were pretrained with the RandAugment (Cubuk et al., 2020) data augmentation method. The following pseudo-code shows data preprocessing for Noisy Student:

```
image = random_flip_left_right(image)
image = random_crop(image)
image = randaugment(image)
```

The randaugment(.) method applies a set of 14 augmentations including ['AutoContrast', 'Equalize', 'Invert', 'Rotate', 'Posterize', 'Solarize', 'Color', 'Contrast', 'Brightness', 'Sharpness', 'ShearX', 'ShearY', 'TranslateX', 'TranslateY', 'SolarizeAdd']

SWAG: We use three SWAG models (Singh et al., 2022). These model were pretrained using weakly supervised pretraining on more than 3.6 billions Instagram images. The pretraining dataset was labeled with hashtags and have 27K classes. We use SWAG-ViT-L, SWAG-ViT-H, and SWAG-RegNetY.

MLP-Mixer: We use two models with MLP-like architectures. These are MLP-Mixer-B/16 and MLP-Mixer-L/16 introduced in (Tolstikhin et al., 2021).

B.3 Model Sources

All the models checkpoints we use are in PyTorch format. The models are from seven main sources. These sources are Pytorch Image Model library (timm), the official CLIP repository, PyTorch Pretrained ViT repository, ptrnets repository, Hugging Face Transformers library, Torchvision, and Torch Hub. Table (1) shows the source of each model we use.

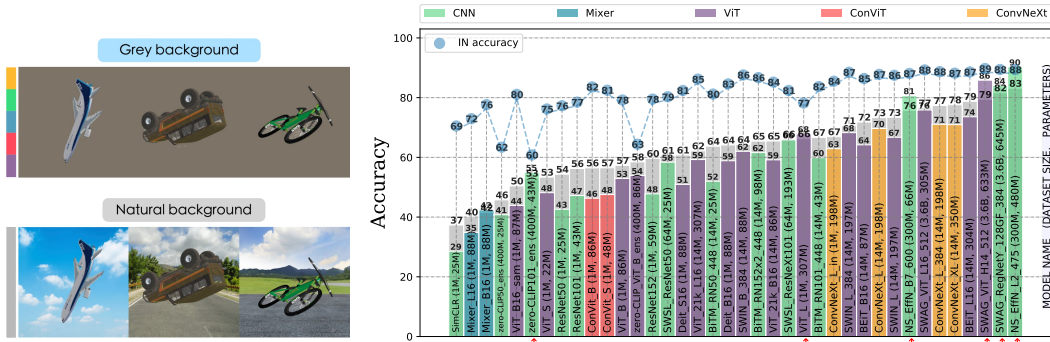
Table 1: **Models details:** The full list of models. Here we report the ImageNet accuracy mentioned in the papers, unless a different accuracy score is provided with the implementation we use. Some model were tested with input resolution higher than the standard 224x224 resolution, in this case the input resolution is added after the model name.

Model	Source	Data	Size(M)	IN
Resnet50	torchvision	ImageNet(1M)	25M	76.1%
Resnet152	torchvision	ImageNet(1M)	69M	77.3%
Resnet101	torchvision	ImageNet(1M)	43M	78.3%
CLIP-ViT-B16	CLIP	WT(400M)	86M	63.2%
CLIP-RN50	CLIP	WT(400M)	25M	62.2%
CLIP-RN101	CLIP	WT(400M)	43M	59.6%
ViT-L16	timm	ImageNet(1M)	307M	77%
ViT-B16	timm	ImageNet(1M)	86M	78%
ViT-S16	timm	ImageNet(1M)	22M	75%
ViT-B16-sam	timm	ImageNet(1M)	86M	79.9%
ViT-21k-B16	pretrained-vit	ImageNet21k(14M)	86M	84%
ViT-21k-L16	pretrained-vit	ImageNet21k(14M)	307M	85%
SWIN-B-384	timm	ImageNet21k(14M)	88M	86.4%
SWIN-L	timm	ImageNet21k(14M)	197M	86.3%
SWIN-L-384	timm	ImageNet21k(14M)	197M	87.3%
Simclr	timm	ImageNet(1M)	25M	68.9%
BiTM-RN50	timm	ImageNet21k(14M)	25M	80.0%
BiTM-RN101	timm	ImageNet21k(14M)	43M	82.5%
BiTM-RN152x2	timm	ImageNet21k(14M)	98M	85.5%
SWSL-ResNet50	torchhub	(64M)	25M	79.1%
SWSL-ResNeXt101	torchhub	(64M)	193M	81.2%
Mixer-B16	timm	ImageNet(1M)	59M	76.44%
Mixer-L16	timm	ImageNet(1M)	207M	71.76%
BEiT-B16	transformers	ImageNet21k(14M)	87M	85.2%
BEiT-L16	transformers	ImageNet21k(14M)	304M	87.4%
DeiT-B16	timm	ImageNet(1M)	86M	83.4%
DeiT-S16	timm	ImageNet(1M)	22M	81.2%
EffN-B7-NS	torchhub	JFT(300M)	66M	86.9%
EffN-L2-NS	torchhub	JFT(300M)	480M	88.4%
ConvNeXt-XL	timm	ImageNet21k(14M)	350M	87.0%
ConvNeXt-L-384	timm	ImageNet21k(14M)	198M	87.5%
ConvNeXt-L	timm	ImageNet21k(14M)	198M	86.6%
ConvNeXt-L	timm	ImageNet21k(1M)	306M	82.6%
ConVit-B	timm	ImageNet(1M)	86M	82.4%
ConVit-S	timm	ImageNet(1M)	27M	81.3%
SWAG-ViT-L16-512	torchhub	IG(3.6B)	305M	88.07%
SWAG-ViT-H14-512	torchhub	IG(3.6B)	633M	88.55%
SWAG-RegNetY-128GF-384	torchhub	IG(3.6B)	645M	88.23%

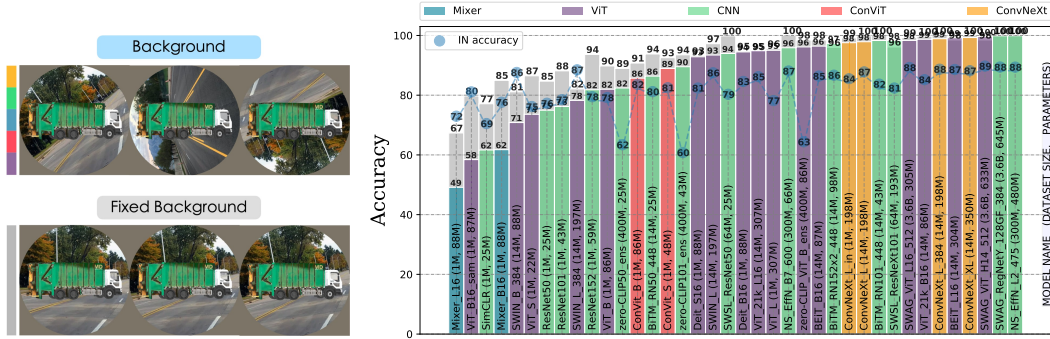
C Additional Experiments

C.1 Effects of the Background Image

To better understand the reliance of different networks on the background image in taking decision, we conduct additional analysis. We find that removing the background and replacing it with grey background harms most of the models on ObjectPose (Fig. 13.A). However, for the strong models this results in improving the model’s performance. In addition, we study the effect of rotating the background image while keeping the foreground object upright (Fig. 13.B). We observe that the strong models on ObjectPose are not affected by rotating the background when the object is upright, while the weak models show some performance degradation. This supports the result mentioned in section 3 that the weak models rely on different strategies than the strong models regarding exploitation of the background image.



(A) ObjectPose: Natural vs Grey Background



(B) Effect of rotating the background

Figure 13: (A) Effect of removing the background image on accuracy. Models are sorted by their accuracy on a natural background. Removing the background impairs performance for most models, but it increases performance for the best models, revealing a different strategy used by these models. (B) Effect of rotating the background image on accuracy, when keeping the object upright. Models are sorted by their accuracy on a rotated background. The best models are unperturbed by this manipulation, again revealing a difference in strategy with the smaller models.

C.2 Additional Experiments with CLIP

The natural language supervision of CLIP using a very large dataset (400M) gives zero-shot CLIP the ability to generalize to many datasets. This helps CLIP-ResNet-101 and CLIP-ViT-B/16 achieve accuracy close to their ImageNet accuracy on ImageNetV2, CO3D dataset, and ObjectPose +10 datasets. However, on ObjectPose, the performance of these models drops as shown in Fig. 7 and Fig. 15. To measure the ability of CLIP models to benefit from the information in the prompt to detect objects in unusual poses (ObjectPose), we tested three CLIP models (CLIP-ResNet-50, CLIP-ResNet-101, and CLIP-ViT-B/16) with three different prompt choices: (1) single general prompt, this is a single prompt proposed by CLIP paper ("a photo of a <class name>"), (2) 80

general ImageNet prompts, these are 80 prompts proposed by the paper for the ensembling over multiple zero-shot predictions for ImageNet (results reported in the main text), (3) 12 prompts we customized for ObjectPose by adding a word that indicates that the object is rotated such as "flipped", "rotated", "upside-down", etc. We find that ensembling ObjectPose-customized prompts improves the performance on ObjectPose. The result in Fig. 14 shows that the 12 ObjectPose-customized prompts are better than the 80 general prompts on ObjectPose. This indicates that CLIP benefits from the information provided in the prompts telling that the object in the images is flipped. This is in contrast to ObjectPose +-10 where the ObjectPose-customized prompts become misleading and give lower accuracy than the general prompts but still better than the single prompt.

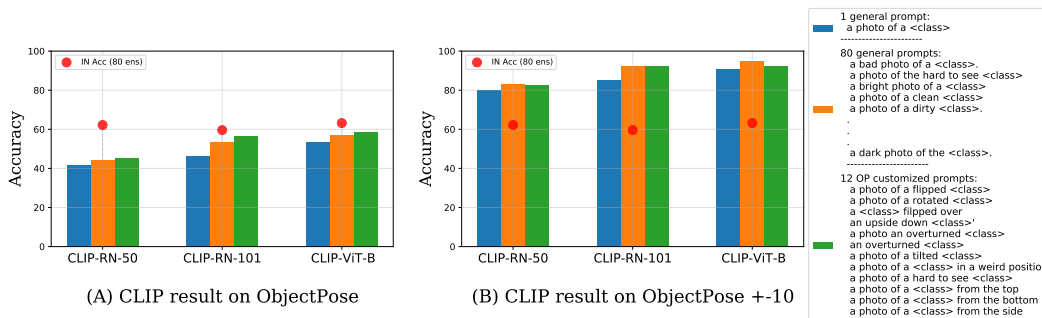


Figure 14: **How prompt engineering and ensembling affect CLIP performance for both ObjectPose and ObjectPose +-10 (upright objects).** For the ObjectPose customized prompts, we inject the information that the object is rotated through the prompts. The legend shows all 12 customized prompts. **(A)** On ObjectPose, the customized prompts outperform both the single prompt and the ensemble of the 80 general prompts. **(B)** When the object is upright (ObjectPose +-10) the customized prompts become misleading and the general prompts perform better.

C.3 The Relationship Between ImageNet Accuracy and OOD Accuracy: The OOD robustness on ImageNetV2 and CO3D does not always transfer to robustness on ObjectPose

Prior studies (Taori et al., 2020) (Miller et al., 2021) show that in-distribution performance correlates strongly with out-of-distribution generalization performance for a wide range of models, tasks, and distribution shifts. Fig. 15 shows the relationship between the accuracy on ImageNet and the accuracy on the OOD datasets we are testing (ImageNetV2, CO3D, and ObjectPose). The figure shows that as we move from ImageNetV2, to CO3D, to ObjectPose, the accuracy relationship starts to deviate from the ideal correlation (when the OOD accuracy equals the in-distribution accuracy) for most of the models except the ones pretrained on large datasets (EfficientNet-L2, and SWAG). This proves that OOD robustness on ImageNetV2 and CO3D does not always transfer to robustness in detecting objects in unusual poses (ObjectPose). We observe also in Fig. 15 that the weak ImageNet models suffer from a higher accuracy drop on CO3D and ObjectPose compared to the stronger ImageNet models.

C.4 Two-axes Rotation

To further assess the models' robustness to unusual poses we created a set of images by rotating the 3D object along two axes. We picked the two axes to be the *ROLL* and *PITCH* axes orthogonal to the 3D object. We rotate the object 10 times along each axis by increasing the rotation angle by 36° each time. This generates 100 images in total for each 3D object. Figures 18-24 shows the predictions on these 100 images by two models (EfficientNet and BiT) for some objects. Although these models achieve high in-distribution performance, they are still making many mistakes on images that seems easy for the human.

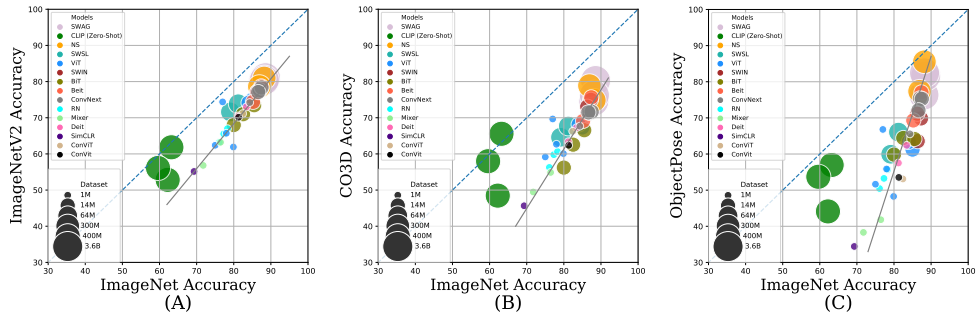


Figure 15: Networks’ accuracies on ImageNet vs ImageNetV2, vs CO3D and vs ObjectPose. The dotted line corresponds to the ideal case when the OOD performance equals the in-distribution performance. CLIP models almost fit the dotted line on ImageNet and CO3D, but their performance degrade on ObjectPose. (A) On **ImageNetV2**, all the models lie below the dotted line, but they follow a line parallel to it (the grey line). The percentage of progress on ImageNet results in the same percentage of progress on ImagenetV2 for all the models. (B) On **CO3D**, the grey line starts to deviate from the dotted line. The weak models’ accuracy transfers to OOD accuracy with less percentage than the stronger models. (C) On **ObjectPose**, the grey line deviates further from the ideal line. The best ImageNet models are less affected by the object poses than the weak models. Fig. 16 provides more comparisons.

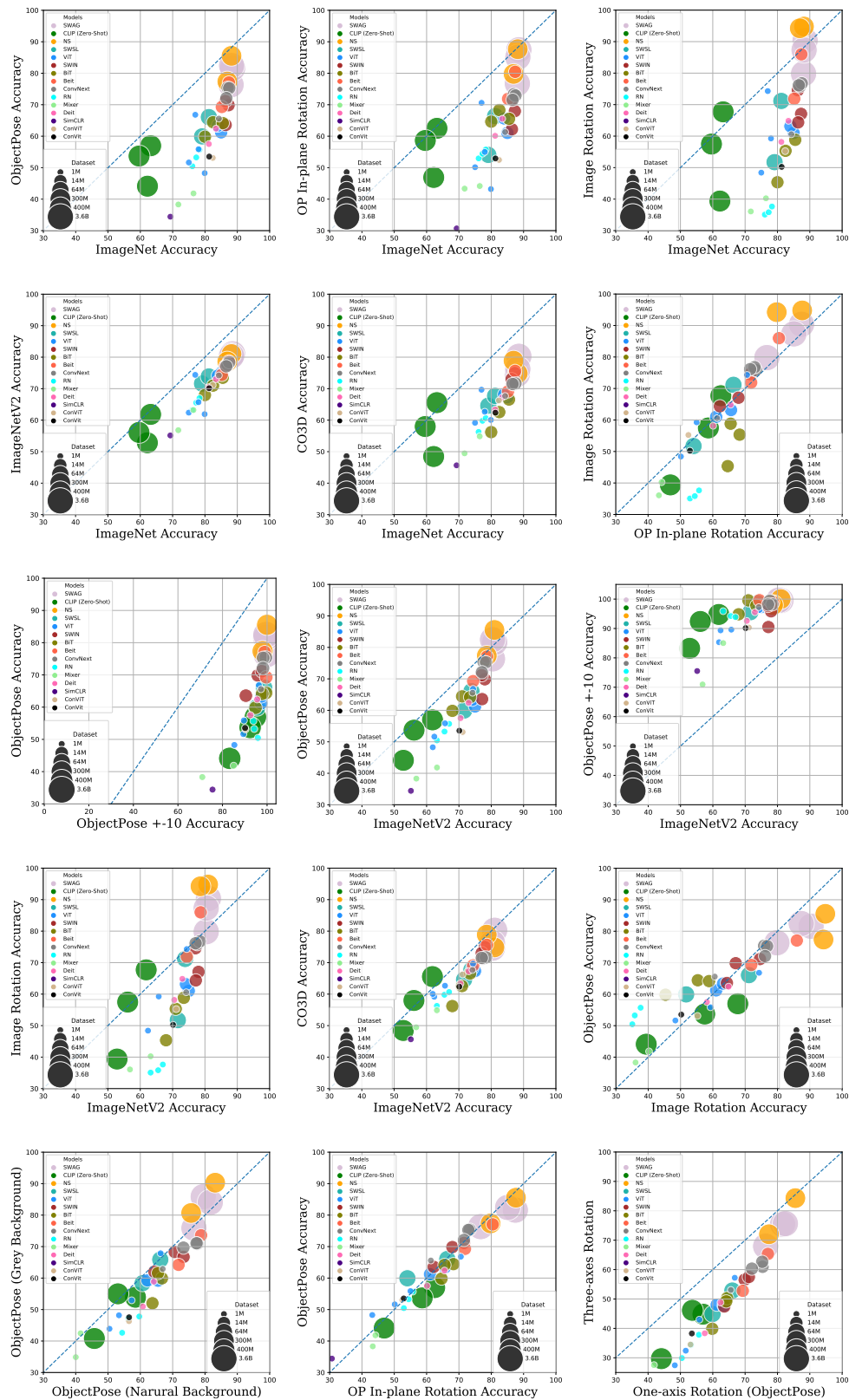


Figure 16: Correlations between the performance of 38 models on the different datasets (ImageNet, ObjectPose, ObjectPose +-10, ImageNetV2, and CO3D).

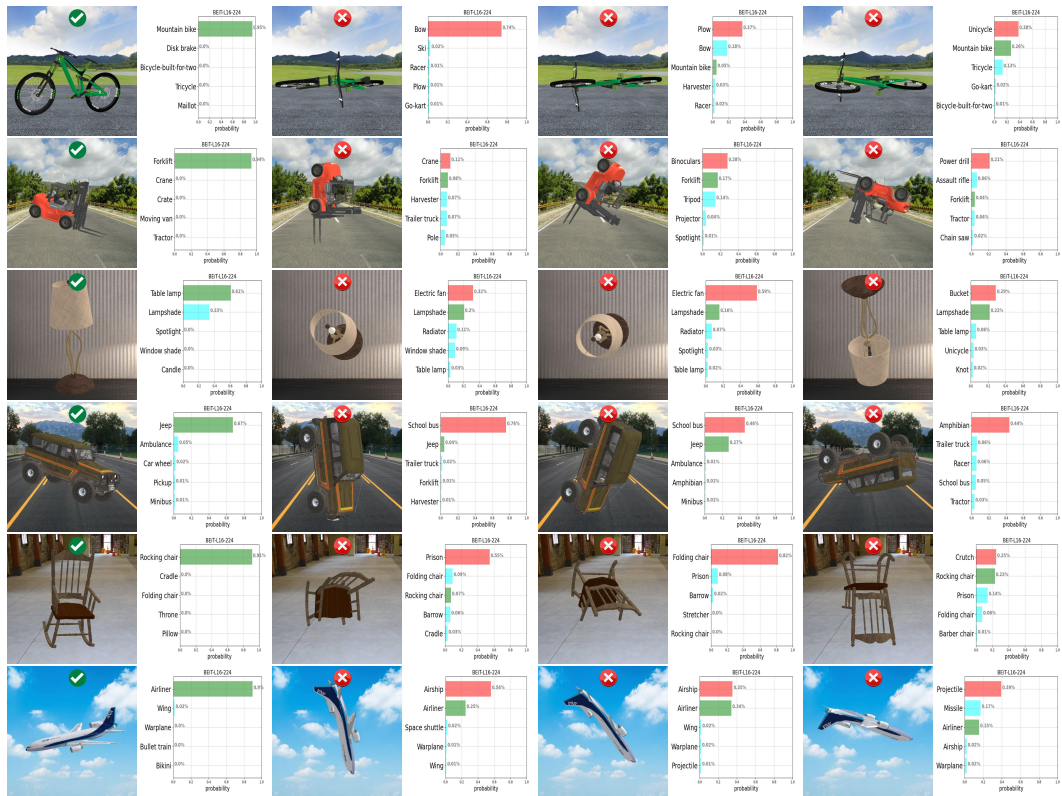


Figure 17: Selected errors made by BEiT-L/16 on the ObjectPose dataset.

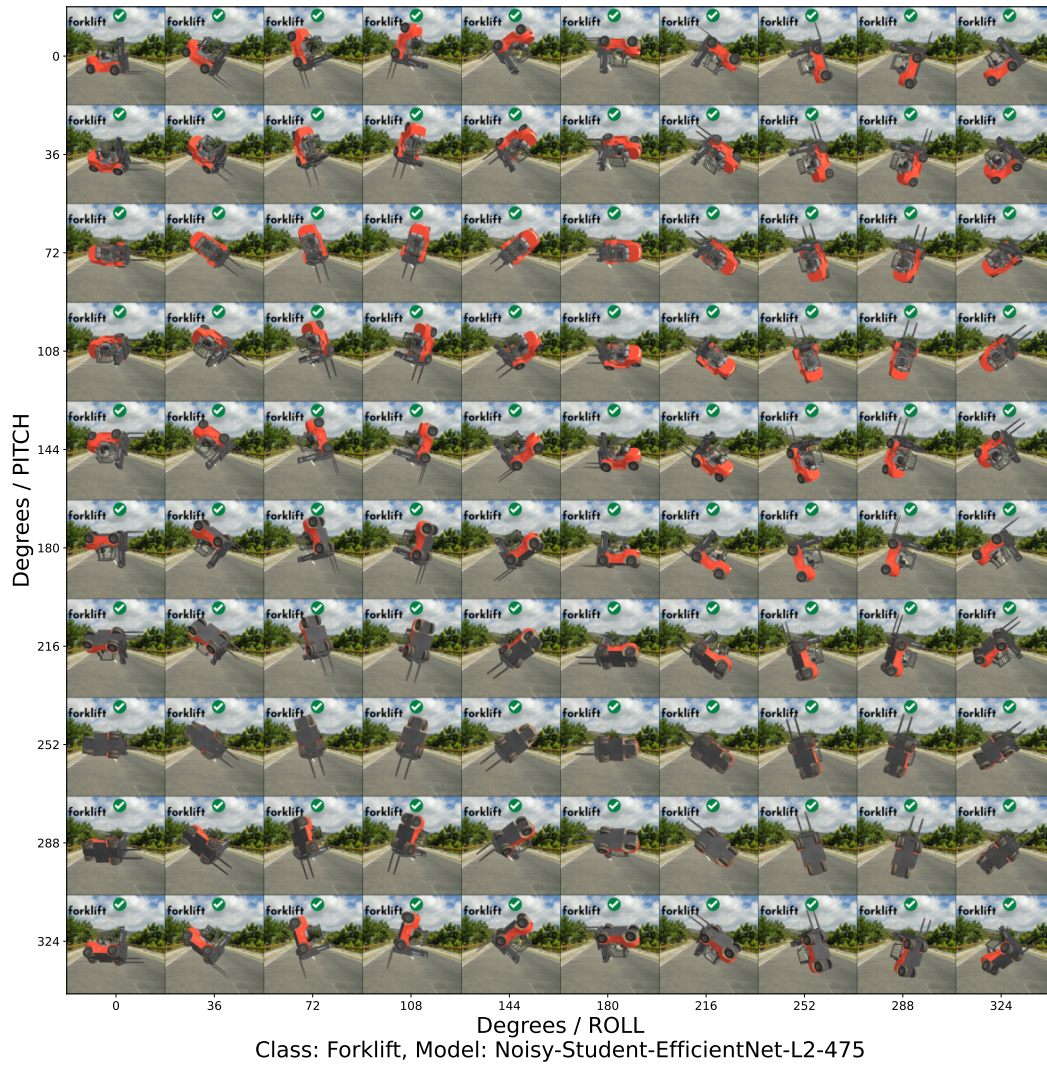


Figure 18: Noisy Student EfficientNet-L2 predictions on two-axes rotations of a forklift. Impressively, the model is able to classify all images perfectly.

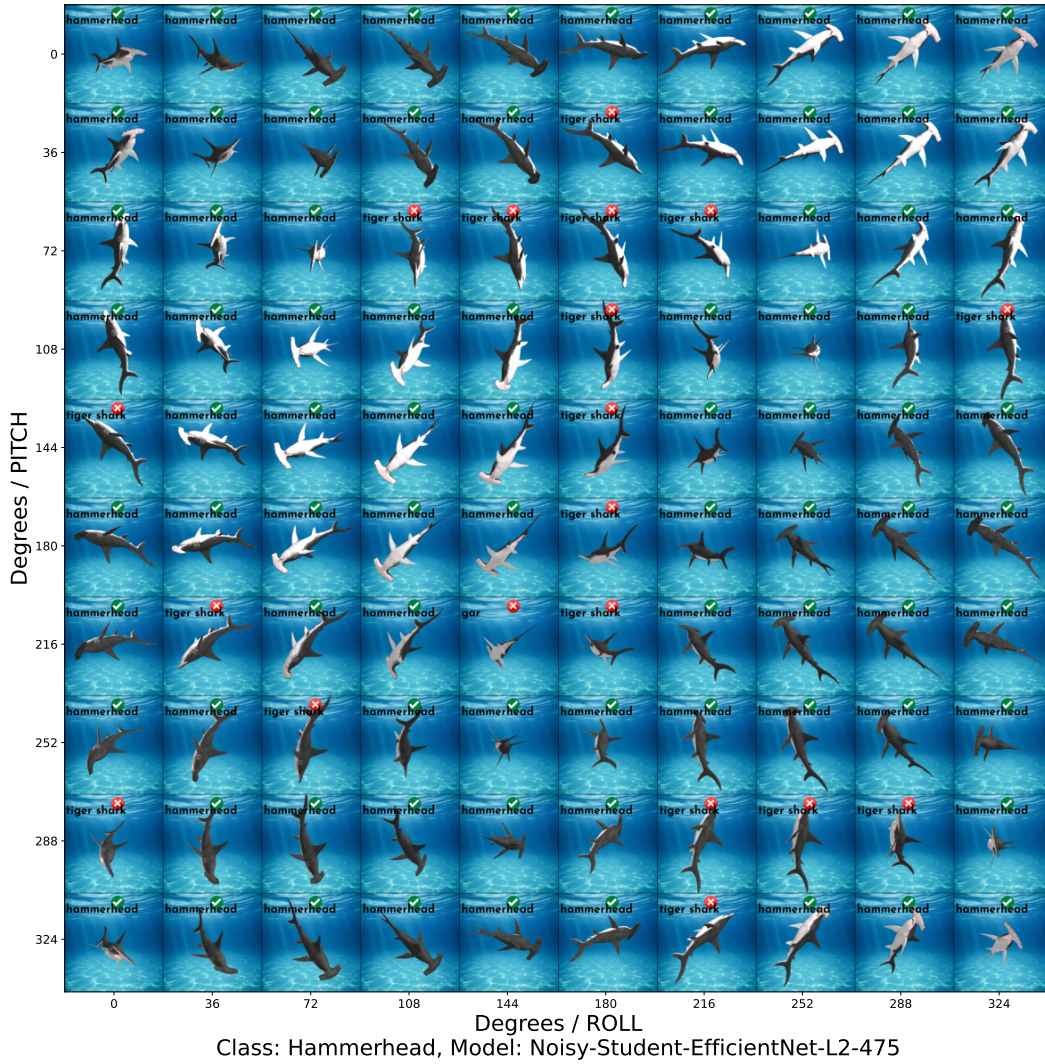


Figure 19: Noisy Student EfficientNet-L2 confuses a hammerhead shark with a tiger shark for poses where the hammerhead is invisible or barely visible. This is an error a human could easily do.

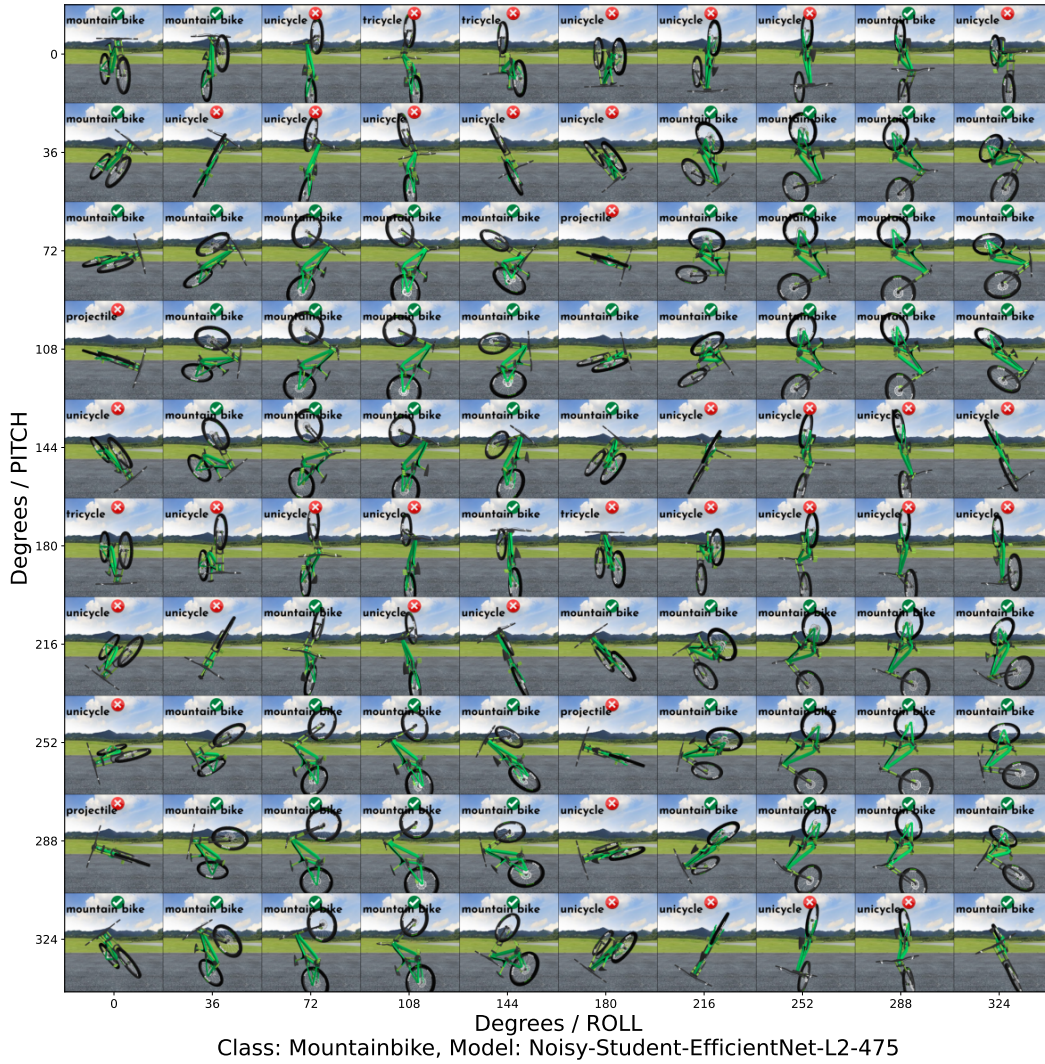


Figure 20: Noisy Student EfficientNet-L2 predictions on the two-axes rotation images of a mountain bike. The model confuses the bicycle with a tricycle or a unicycle for some unusual poses.

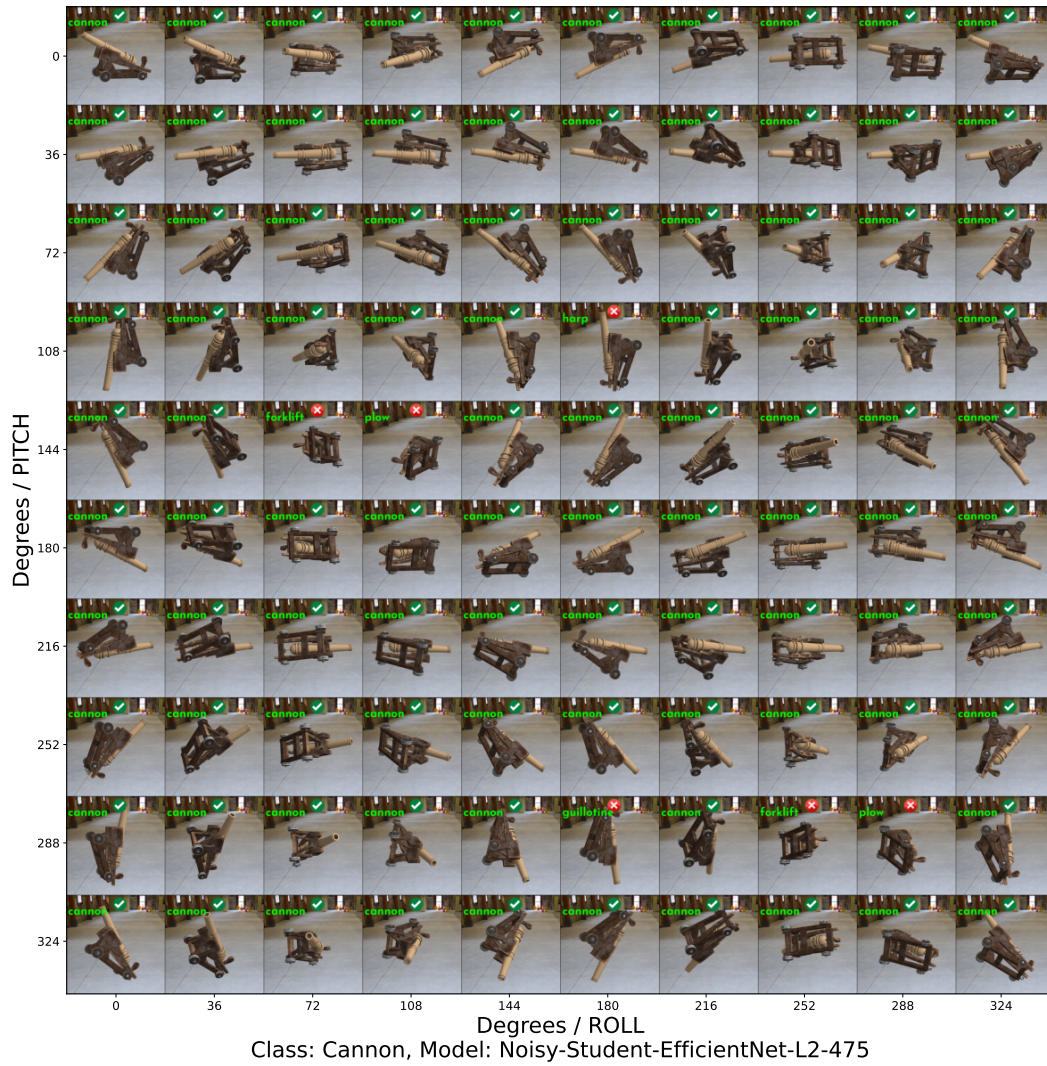


Figure 21: Noisy Student EfficientNet-L2 confuses a cannon with a harp or a guillotine when it is at 90° from the upright position. This is an error that a human would probably not do.

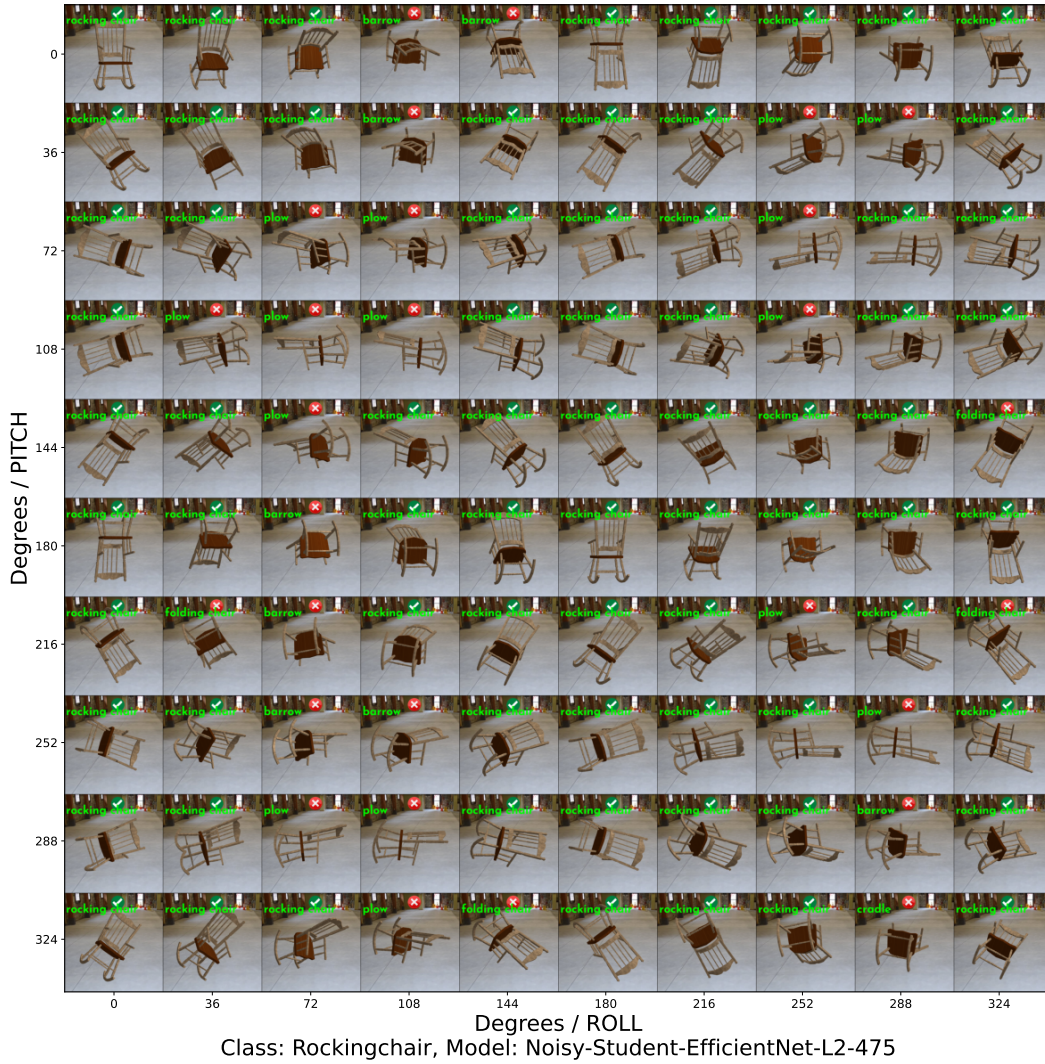


Figure 22: Noisy Student EfficientNet-L2 predictions on two-axes rotations of a rocking chair. The model makes some mistakes in classifying some of the rocking chair images.

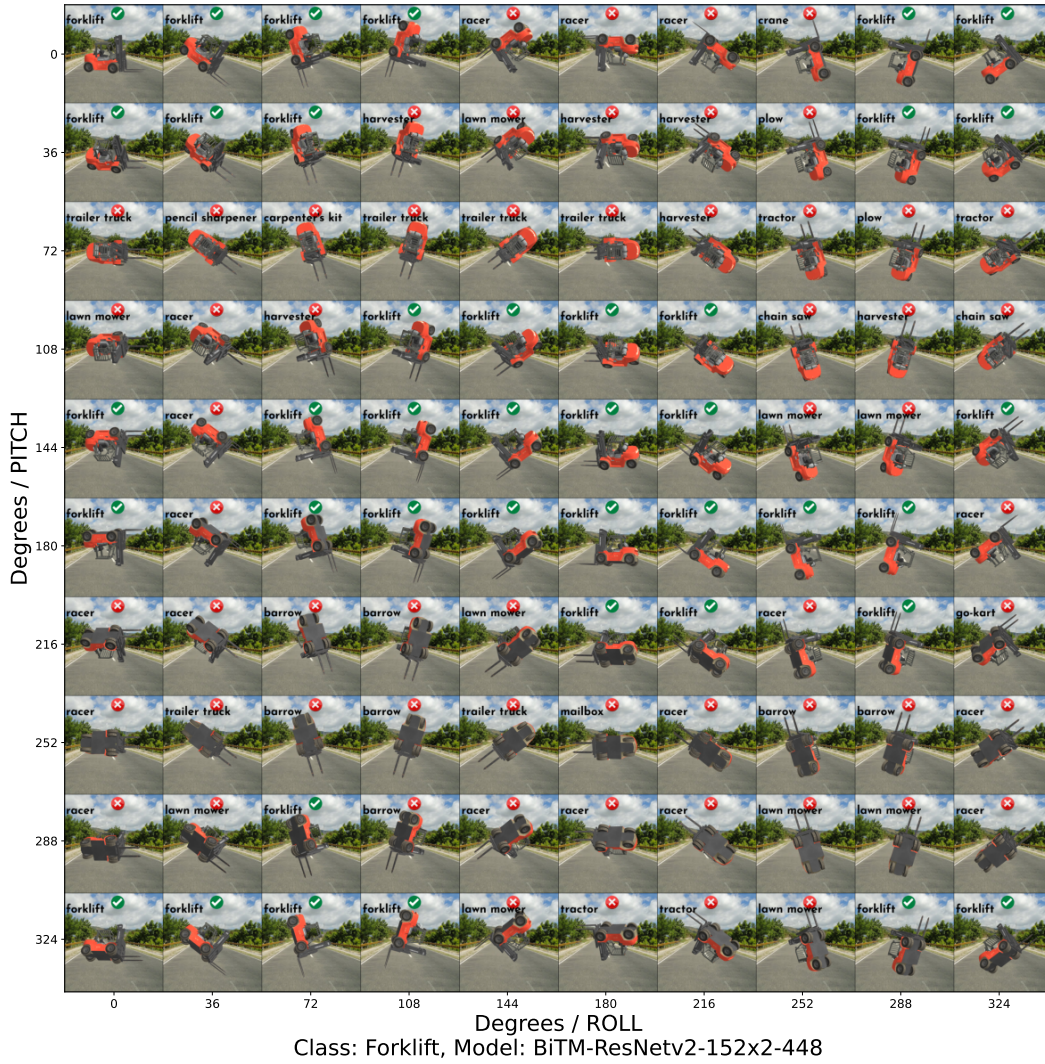


Figure 23: BiTM predictions on two-axes rotations of a forklift. This model is much less robust than larger models such as Noisy Student EfficientNet-L2.

